LDHs BASED NANOSORBENTS FOR REMOVAL OF ANIONIC DYES

BY

TAYE SAHEED KAZEEM

A Thesis Presented to the

DEANSHIP OF GRADUATE STUDIES

KING FAHD UNIVERSITY OF PETROLEUM & MINERALS

DHAHRAN, SAUDI ARABIA

In Partial Fulfillment of the
Requirements for the Degree of

MASTER OF SCIENCE

In

CHEMICAL ENGINEERING

DECEMBER 2017

KING FAHD UNIVERSITY OF PETROLEUM & MINERALS

DHAHRAN- 31261, SAUDI ARABIA

DEANSHIP OF GRADUATE STUDIES

This thesis, written by **TAYE SAHEED KAZEEM** under the direction of his thesis advisor and approved by his thesis committee, has been presented and accepted by the Dean of Graduate Studies, in partial fulfillment of the requirements for the degree of **MASTER OF SCIENCE IN CHEMICAL ENGINEERING.**

17-4-18

Dr. Mamdouh Al-Harthi
(Advisor)

Dr. Mohammed Ba-Shammakh
Department Chairman

16-4-2018

Dr. Abdulhadi Al-Juhani
(Member)

Dr. Salam A. Zummo
Dean of Graduate Studies

16/04/18

Dr. Wasif Farooq
(Member)

1/5/18

Date

16/04/2018

Dr. Umer Zahid
(Member)

16/04/2018

Dr. Muhammad Shahzad Kamal
(Member)

I dedicate this work to my loving grandmother and my beautiful wife for their commitment to my success.

ACKNOWLEDGMENTS

All praise and adoration is due to Almighty God for his mercy and blessings to see me through the journey of my M.Sc. study. I seek the peace and mercy of Almighty Allah upon the noble prophet Muhammad.

I will like to appreciate my family for their support during this period especially my wife for standing by me and encouraging me. I want to say a big thank you for my supervisor Dr. Mamdouh Al-Harthi for his fatherly role, believing in me and providing me more insight to horn my research skills. I want to appreciate my awesome committee for their contribution towards the completion of this work. I appreciate my friend Musa Najimu for his continuous words of encouragement. I want to also acknowledge the Nigeria community, NCUPM, at KFUPM for their support. I will like to further acknowledge the department of Chemical Engineering, KFUPM for their great faculty members and staff for their enormous support.

Lastly my appreciation goes to KFUPM and the kingdom of Saudi Arabia for providing me the privilege and platform to complete a graduate study. All in all, thank you everyone for being part of this beautiful phase of mine.

TABLE OF CONTENTS

LIST OF TABLES

LIST OF FIGURES

LIST OF ABBREVIATIONS

EBT	:	Erichrome Black T
FTIR	:	Fourier Transform Infrared
G/MCA	:	Graphene Magnesium Cobalt Aluminium LDH nanocomposite
G/MCA-C	:	Calcined Graphene Magnesium Cobalt Aluminium LDH nanocomposite
G/NMA	:	Graphene Nickel Magnesium Aluminium LDHs nanocomposite
G/NMA-C	:	Calcined Graphene Nickel Magnesium Aluminium LDH nanocomposite
LDHs	:	Layered Double Hydroxides
MCA	:	Magnesium Cobalt Aluminium LDH
MCA-C	:	Calcined Magnesium Cobalt Aluminium LDH
MMO	:	Mixed Metal Oxide
MO	:	Methyl orange
NMA	:	Nickel Magnesium Aluminium LDH
NMA-C	:	Calcined Nickel Magnesium Aluminium LDH
TGA	:	Thermogravimetry analysis
SEM	:	Scanning Electron Microscopy
XRD	:	X-Ray Diffraction

ABSTRACT

Full Name : Taye Saheed Kazeem

Thesis Title : **LDHs Based Nanosorbents For Removal of Anionic Dyes**

Major Field : Chemical Engineering

Date of Degree : December 2017

Dyes are continuous global demanded products and are majorly disposed in water bodies; thus, the treatments of such pollutants are major challenges. Adsorption among various treatment options is affordable and available which endear its use by researchers and treatment plants. Of the various adsorbents used and reported, layered double hydroxides (LDHs) has been found to possess outstanding properties such as high surface area and excellent ion exchange capacities as well as ease of synthesis and regeneration.

The focus of this work lies on the synthesis of Ternary layered double hydroxide, NiMgAl (NMA) and MgCoAl (MCA) LDH, and their graphene based nanocomposites (G/NMA and G/MCA) via coprecipitation technique. These nanomaterials and their calcined products NiMgAl LDO (NMA-C), MgCoAl LDO (MCA-C), Graphene-NiMgAl LDO (G/MCA-C) and Graphene-NiMgAl LDO (G/NMA-C) were then used for the removal of an anionic dyes, Eriochrome Black T (EBT) and Methyl orange (MO), from aqueous solution. The adsorption processes were studied through isotherm, kinetic and thermodynamic investigations of various parameters such as initial solution pH, contact time, adsorbent dosage, initial dye concentration and temperature. All the adsorbent samples exhibit fast sorption optimized at acidic pH due to abundance of oxygen containing functional groups. The adsorption processes were suitably fitted by Langmuir isotherm with maximum adsorption computed to be 384.62 mg/g for EBT adsorption on G/NMA-C

and 434.78 mg/g for adsorption of MO on G/NMA-C. The highest capacities obtained for the calcined graphene nanocomposites arise from the synergistic contribution of graphene integration and calcination.

Furthermore, kinetics evaluation showed the suitability of pseudo-second order model which is due to the chemisorption nature of the adsorption process. Thermodynamics study has revealed the exothermic nature of the adsorption processes. High removal efficiency of the dyes with better recovery and reusability of these nanomaterials has highlighted their potential application in toxic water remediation.

ملخص الرسالة

الاسم الكامل: تايى سعيد كاظم

عنوان الرسالة: LDHs استنادا نانو المواد الماصة لإزالة الأصباغ الأنيونية

التخصص: هندسة كيميائية

تاريخ الدرجة العلمية: كانون الأول 2017

لأصباغ هي منتجات مطلوبة عالمية مستمرة ويتم التخلص منها بشكل رئيسي في المسطحات المائية. وبالتالي ، فإن معالجات هذه الملوثات تشكل تحديات رئيسية. الامتزاز بين خيارات العلاج المختلفة هو بأسعار معقولة ومتاحة والتي تحرص على استخدامها من قبل الباحثين ومحطات العلاج. من مختلف المواد الممتزّة المستخدمة والمبلّغ عنها ، تم العثور على هيدروكسيد مزدوج الطبقات (LDHs) يمتلك خصائص بارزة مثل مساحة السطح العالية والقدرات الممتازة للتبادل الأيوني وكذلك سهولة التجميع والتجديد.

ينصب تركيز هذا العمل على توليف هيدروكسيد مزدوج الطبقات الثلاثية ، NiMgAl (NMA) و MgCoAl LDH (MCA) ، ومركباتها النانوية المعتمدة على الجرافين (G / NMA و G / MCA) عن طريق تقنية الترسيب. تم بعد ذلك استخدام هذه المواد النانوية ومنتجاتها المكلسة NiMgAl LDO (NMA-C) ، و MgCoAl LDO (MCA-C) ، و Graphene-NiMgAl LDO (G / MCA-C) ، و Graphene-NiMgAl LDO (G / NMA-C) إزالة الأصباغ الأنيونية ، اريوتشروم بلاك تي(EBT) وبرتقال الميثيل (MO)، من محلول مائي. تمت دراسة عمليات الادمصاص من خلال تحليل متساوي للحرارة والحركية والديناميكا الحرارية لمختلف العوامل مثل درجة الحموضة الأولية ، وقت التماس ، الجرعة الممتزة ، تركيز الصبغة الأولي ودرجة الحرارة. تظهر جميع العينات الممتزة امتصاصًا سريعًا محسّنًا عند الأس الهيدروجيني الحمضي بسبب وفرة الأكسجين المحتوية على مجموعات وظيفية. م تجهيز عمليات الامتزاز بشكل مناسب من قبل متساوي الساق لانجمير مع الحد الأقصى من الامتزاز المحسوب ليكون 384.62 ملغم / غرام من أجل امتصاص EBT على G / NMA-C و 434.78 ملغم / جم من أجل امتزاز MO على G / NMA-C. أعلى القدرات التي تم الحصول عليها لمركب نانوي الجرافين المكلس تنشأ من المساهمة التآزرية لتكامل الجرافين والتكليس.

وعلاوة على ذلك ، أظهر تقييم حركية مدى ملاءمة نموذج الطلب الثاني الزائف الذي يرجع إلى طبيعة امتصاص كيميائي لعملية الامتزاز. كشفت دراسة الديناميكا الحرارية الطبيعة الطاردة للحرارة لعمليات الإدمصاص. وقد أبرزت كفاءة إزالة الأصباغ العالية مع تحسين الاستعادة وإعادة القابلية لهذه المواد النانوية إمكانية تطبيقها في معالجة المياه السامة.

CHAPTER 1

INTRODUCTION

More than 700,000 tonnes of dyes are produced worldwide and about 15% of them find way into water bodies as effluents [1, 2]. Azo dyes are one of the world most demanded product due to their extensive use in textiles, printing, paints, plastic and they account for more than 60% of total world dye usage [3]. Organic pollutants are one of the major contributor to the bio-toxic, carcinogenic and anti-aesthetic threats facing human, atmosphere, and hydrosphere existence [4]. The output of these pollutants has been at alarming rate in recent years and there is need for development of abatement schemes to mitigate these daring effects. Wastewater mostly houses dyes at the end of the process. Since time immemorial, dye wastewater treatment and purification has always proven to be an arduous task.

Attempt to mitigate the quantity of these toxic discharge to the environment has led to deployment of treatment schemes such as solvent extraction, ion-exchange, membrane filtration, evaporation, etc. for waste water treatment. These different techniques have relative advantages but their drawbacks such as being expensive, availability, generation of secondary waste as well as regeneration/recyclability has generated concerns. Adsorption processes has shown promises to overcome these challenges with merits such as facile operation, affordability, availability, and efficiency[5-9].

For efficient performance in adsorption, selection and fabrication of the right adsorbent is critical. Adsorbents to considered should be environmentally-affable, affordable, stable and efficient. Despite numerous studies involving adsorption of contaminants from wastewater, the development of adsorbents who are highly recyclable, cheaply fabricated and have high adsorption capability accompanied by high specific surface area is a pivotal topic[10].

Recently, layered double hydroxides (LDHs), also termed as hydrotalcites, has seen huge applications in adsorption processes due to their exceptional ion exchange capacity [11, 12]. LDHs has also been explored in biomedicine, catalysis, magnetization, polymerization, electrochemistry, wastewater treatment, electronics and supercapacitors [12-16].. Furthermore, regeneration and reuse of the spent adsorbent is easy and its performance is comparable with unused LDHs adsorbent[10].

1.1 Aim of Study

This thesis aims at application of LDHs based Nano-sorbents and its nanocomposites for the removal of anionic dye such as Eriochrome Black T (EBT) and Methyl orange (MO) and investigate various factors influencing the dyes adsorption for optimum performance.

1.2 Objectives

Significant studies have gone into studies and applications of LDHs but a lot more still needs to be done. Specifically, we need to further explore the deployment of LDHs in the elimination of anionic dyes from aqueous phases as well as optimizing the factors needed

for efficient removal. To accomplish this, the objectives for this MSc research are highlighted below:

(1) Synthesis of ternary LDHs and Graphene/ternary LDH nanocomposites.

(2) Characterization of the as-synthesized adsorbents.

(3) Study the performance of ternary LDH in removing EBT and MO from aqueous solution.

(4) Study the efficiency of use of Graphene/ternary LDH nanocomposite in removing EBT and MO from aqueous solution.

(5) Determination of appropriate kinetic models describing the adsorption of the dye.

(6) Determination of appropriate adsorption isotherm describing the adsorption of the dye.

(7) Determination of adsorption mechanism of the dye on the LDHs

(8) Regeneration and reuse of adsorbents

CHAPTER 2

LITERATURE REVIEW

2.1 Structural Features

LDHs derived from parent mineral $Mg_6Al_2(OH)_{16}CO3.4H_2O$ [15] is a member of the family of 2-D nanostructured anionic clays which possesses hydrotalcite morphology and characterized by a positively charged host and charge balanced by substitutable interlamellar anions (see **Fig 2.1**). LDHs possesses a unique structural formula of $[M^{2+}_{(1-X)} M^{3+}_{(X)} (OH)_2]^{X+}[A^{n-}]_{X/n}$. mH2O [13] where M^{2+} represents the divalent cations such as Mn^{2+}, Ca^{2+},Co^{2+}, Zn^{2+} , Fe^{2+}, Ni^{2+}, Mg^{2+} while the M^{3+} represents the trivalent cation such as Fe^{3+}, $Al^{3+}$and the A^{n-} is the intercalating anions which can be OH^-, F^-, NO^{3-} , Cl^-, CO_3^{2-} or SO_4^{2-} and n has been reported to lie between 0.22 and 0.33 [15, 17]. Apart from the M^{2+}/ M^{3+} combination of LDHs, quaternary LDHs [18] as well as LDHs with monovalent lithium (with Aluminum as the trivalent cation) are available [19]. There have studies relating to the synthesis of M^{2+}/ M^{4+} combination of LDHs. The range of possible combination of M^{2+}, M^{3+} and A^{n-} as well as variation of ratio of M^{2+} to M^{3+} influence both the ion exchange capacity and charge density of LDHs give rise to different application of LDHs [20-22].

Due to excellent ionic exchange capability, various LDHs have been synthesized for the sorption of toxic materials. Partial and isomorphic substitutions of M^{2+} with M^{3+} result in excess positive charges which are balanced by interlayered water molecules and anions of

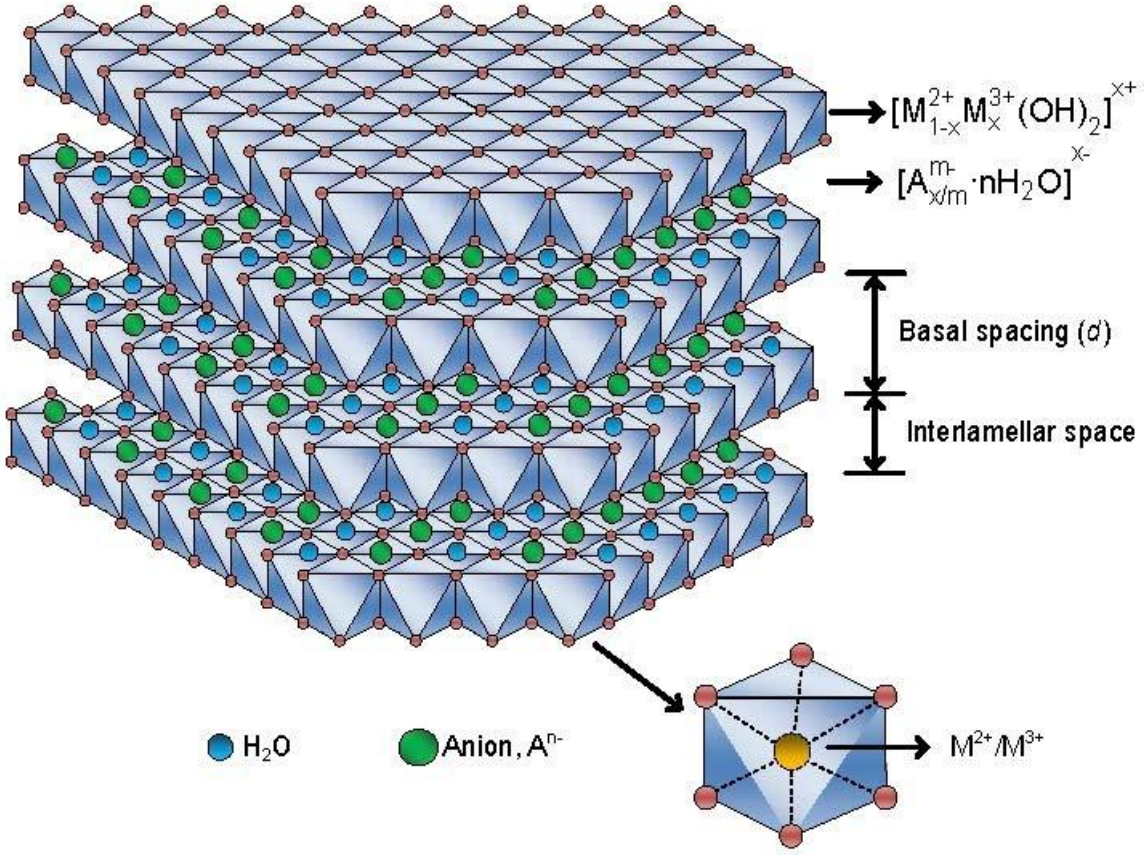

Fig 2.1 Schematic diagram of LDHs

the LDHs[23]. These excellent properties enable LDHs captures both inorganic and/or organic anions. Intercalation of large and highly charged anions into the structure of LDHs provides a great possibility of inducing the adsorption of cations. Heteropoly blue, a derivative of Polyoxometalate, with high negative charge was facilely incorporated by ion-exchange into ZnAl-LDH to eliminate methylene blue in the aqueous mixture [24]. Noticeable shift in the 2θ value is observed in the XRD pattern for a successful intercalation into the LDH structure [24].

2.2 Synthesis of LDHs

LDHs can be facilely prepared through various methods as explained by He et al [25]. These are

2.2.1 Coprecipitation

This involves using precursors of the divalent and trivalent cations to be incorporated into the LDH and preparing under supersaturation condition in order to simultaneously precipitate the cations. The coprecipitation can either be done at high supersaturation or low supersaturation. For high supersaturation, the mixed salt solutions of M^{2+} and M^{3+} is added to alkaline solution possessing the desired intercalated anion. Whereas for low supersaturation, the mixed salt solution is slowly added to the aqueous solution of the required interlayer anion during which alkaline solution is simultaneously added into the reacting mixture to adjust to pH needed for precipitation. Due to formation of larger amount of crystallization nuclei, coprecipitation at high supersaturation produces less crystalline samples compared to low supersaturation.

2.2.2 Rehydration/ Reconstruction

This uses “memory effect” to obtain LDH from mixed metal oxide (MMO). Calcined LDHs, which yield MMO, have the potential to regenerate LDHs on exposure to H_2O and anions[26]. The resultant LDH may also be different from the parent LDH if the introduced anion is different from the anion used in the initial synthesis, hence this is a novel way to synthesis desired LDH tailored for specific application

2.2.3 Nucleation and Aging technique

This synthesis mode was proposed by Zhao et al.[27] in which crystallites formation involves both nucleation and aging and is characterised by rapid mixing. Crystallinity obtained is better than that of coprecipitation.

2.2.4 Ion Exchange

This is applicable when coprecipitation is not feasible which may be due to instability of divalent cation or trivalent cation or anion in alkaline solution. It is also used when direct reaction involving the anion to be intercalated and the host metal is highly favoured. This results in a unique anion-pillared LDH[28]

2.2.5 Urea Hydrolysis

This method have been used in a lot of work for LDHs synthesis [10, 29]. Urea is highly sort after due to its high-water solubility, weak bronsted base nature and facile control of hydrolysis rate.

2.2.6 Hydrothermal

This is more appropriate for intercalating organic guest specie whose affinity is poor for LDHs and where coprecipitation and ion exchange are not feasible. The possibility that the intended organic anion will fill the interlayer position makes this method efficient[30].

2.2.7 Others

one-pot in situ approach [31],Innovative aerogel, fast coprecipitation followed by controlled hydrothermal treatment, secondary intercalation, template synthesis, surface synthesis, salt-oxide method and much more [25]

2.3 Characterization of LDHs

2.3.1 FTIR Spectroscopy Analysis

LDHs are characterised by a variety of vibration which may consist of bending, symmetric stretching and antisymmetric stretching modes of the interlayer water molecules; bending, torsion, symmetric stretching and antisymmetric stretching modes of the carbonate group; stretching modes of the metal-hydroxyl ion bond (M-OH) as well as vibrations of the metal-metal bond (M-M). Usually the peaks between 3200-3800 cm^{-1} is associated with the stretching vibrations of OH group of interlayer H_2O as observed for the 3 calcined LDHs in Zubair et al. [32]. Peaks around 1500-1700 cm^{-1} corresponds to bending vibrations of OH in water molecules while peaks around 1300-1500 cm^{-1} indicates antisymmetric vibrations associated with C=O of carbonate group[33]. Other peaks associated with carbonate are located around 1000-1100 cm^{-1} (bending non-polar mode), 800-900 cm^{-1} (torsion mode), 600-700 cm^{-1} (bending angular mode) [33]. (check notebook to locate reference). The M-O-M, M-O and O-M-O peaks are found below 1000 cm^{-1}[32].

2.3.2 X-Ray Diffraction (XRD)Analysis

XRD pattern of LDH are characterized by typical reflection peaks 003, 006, 009, 110 and 113 spectrums as shown in Fig 2.2. Intense diffraction peak is an indication of good crystallinity while a lower peak indicates poor crystallinity [32, 33]. For composites, which may involve physical deposition of extra specie on the LDH such as Fe_3O_4/ZnCr-LDH composite [34], the reflection peaks may not be change obviously when compared to the individual component.

2.3.3 Scanning Electron Microscopy (SEM)

The morphology, size and composition of LDHs can be explicitly shown by SEM. ZnAl-LDHs of molar ratio of Zn/Al equals 2 displays a hexagonal platelet morphology which changes to a 3D ‘‘silk flower-like” structure on using water–n-BuOH as solvent for synthesis instead of the initially used water [35]. The ZnAl-LDHs morphology was also earlier shown in the work of Zhang et al. [36]. As-synthesized MgAl-LDHs shows hexagonal platelet structure which transforms to a blossom sphere on incorporation of Zn to form ZnMgAl-LDHs [37]. The perfect blossom spherical configuration of the ZnMgAl-LDHs reduces with increase in the Zn/Mg until it almost vanishes at a ratio of 0.8. Zubair et al. [32] reported CoAl-LDHs to display cotton-like agglomerates while MgAl shows irregular cubical morphology while NiFe shows a coarse, rutted flowered like particles.

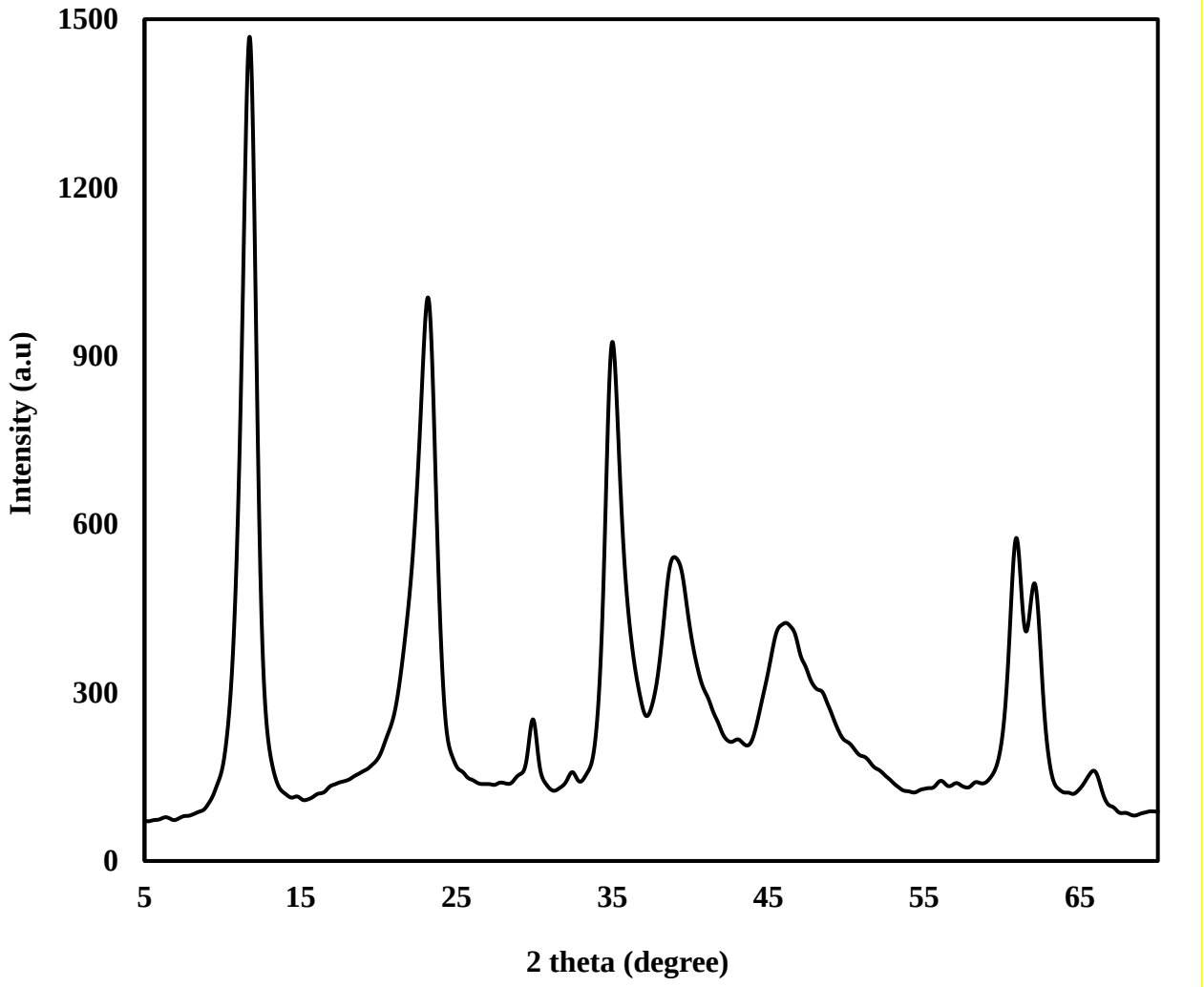

Fig 2.2 Sample XRD of LDHs

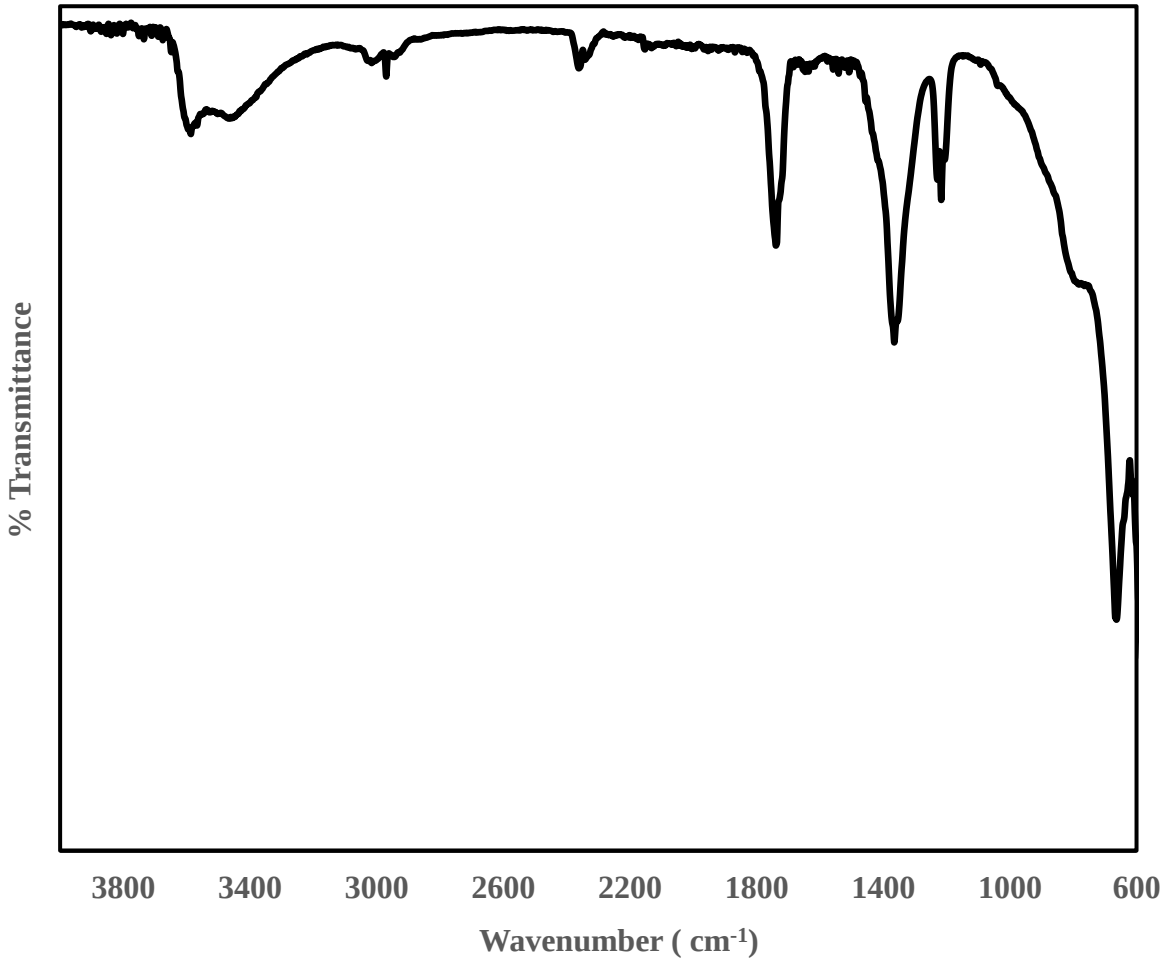

Fig 2.3 Sample FTIR of LDHs

2.3.4 BET-Analysis

This analysis involves documentation of the corresponding pore size distributions (PSD) of the adsorbent carried out by nitrogen adsorption-desorption with a. As shown in table 2.1, LDHs possess high specific surface area. More importantly, calcination improves the specific surface area of LDHs, hence an increase in adsorption capacity. Furthermore, hybrid nanocomposites are characterized by higher surface area and individual components

2.4 Adsorption Mechanism

The mechanism behind adsorption of adsorbates on LDHs adsorbents covers a wide range from ion exchange[38], to electrostatic attraction and chemical/ hydrogen bond between the adsorbent and adsorbate[32]. Also, chemisorption has been reported as the mechanism in the work of Zhi-qing Zhang et al.[29] in the adsorption of Cr(VI). Yasin et al. [39] explained that the mechanism behind Pb^{2+} removal from aqueous solution was surface precipitation reaction for Mg–Al LDH while complex formation was responsible for tartrate intercalated Mg–Al LDH removal of Pb^{2+}. Isomorphic substitution was proposed as one of the possible mechanism for adsorption in removal of Cu(II) during the simultaneous removal of Cr(VI) and Cu(II) ions from aqueous solution[40]. Due to isomorphism between Mg and Cu(II), Cu(II) who possesses slightly larger ionic diameter substituted into the brucite-structure thereby increasing the basal spacing of the resultant LDH. Other removal mechanisms is the work were anion-exchange, precipitate formation of $Cu_2Cl(OH)_3$, and adsorption of Cr(VI) by $Cu_2Cl(OH)_3$.

For anionic Congo Red dye removal using MgAl-Cl LDH, Lafi et al [41] reported surface adsorption as the mechanism as no shift in the ray spectrum of Congo Red adsorbed on LDH (MgAl–LDH-CR) when compared with the MgAl-LDH

Table 2.1 BET Surface Areas of Various LDHs

LDHs	Surface Area (m^2/g)	Pore Volume (mL/g)	Reference
MgAl	24.74 (uncalcined)	---	[42]
	165.07 (calcined)		
TiO_2/ ZnAl	37.3 (ZnAl)	---	[31]
	153.6 (TiO_2/ ZnAl)		
Fe_3O_4/ZnCr	45 (ZnCr)	---	[34]
	114 (Fe_3O_4/ZnCr)		
NiAl	205.76 (calcined)	0.4139	[43]
ZnMgAl	82.13	---	[37]
Fe_3O_4/ZnCr	185.20	---	[44]

2.5 Effects of Various Parameters on Adsorption

2.5.1 pH

The contribution of pH on the removal efficiency of adsorbents ranges from no effects, increasing adsorption to decreasing adsorption with increase in initial pH of the solution. The is due to fact that pH influences the adsorbent surface charge as well as the degree of ionization of adsorbate [41, 45]. An important factor to consider is the pH at Point of zero charge (pH_{pzc}). Cosidering $pH>pH_{pzc}$, LDH surface has a resultant negative charge, which leads to repulsion of the anionic dyes by the LDHs but this favours the adsorption of positive dyes. For $pH < pH_{pzc}$, a positively charged LDH result which favors adsorptions of anionic dyes while unfavourable adsorption occurs for cationic dyes. However, very small value of pH, pH≪pHpzc, the LDH becomes impaired resulting in instability and this reduces the adsorption of anionic dyes. At very high pH ($pH>>pH_{pzc}$), increasing competition of OH^- adsorption for active adsorption sites reduces the adsorption of anionic dyes[15].

For study involving adsorption of Congo red in aqueous medium by MgAl-LDH, the amount removal increases insignificantly with pH increase (in range of 2.7 to 10.2) [41]. This was due to the buffering capability of the LDHs[46, 47]. Beyond this buffering pH range, the adsorption capacity of LDH reduces because of electrostatic repulsion between adsorbate and adsorbent and/ or competition between the anionic adsorbate and OH^- for the active adsorption sites

In the study of Shan et al. [33], no effect of pH increment on one of the dye (RR) where as for the other two (CR and AR1), the adsorption varied negligibly with pH from 2-10 after

which there was a sharp decrease in adsorption with increase in pH. The chemistry between the adsorbent and dye molecules is affected by pH of dye solution. For the study of Yang and his team, the adsorption capacity increases as the pH increases from 2 until a maximum pH of 5[48]. Also, as at the maximum pH, the adsorption performance of the LDHs is greater than the individual building units due to synergistic effects. In addttion, the calcined LDH has higher adsorption performance than the noncalcined counterpart. Adsorption quantity of EBT with increased in pH for all the three LDHs considered in the work of Zubair etal. [32]. This was associated with reduced electrostatic attracion between anionic dye EBT and LDH at higher. The same report was earlier presented by Yasin et al. [49]

Decreasing adsorption with increasing pH was reported in removal of methyl orange by calcined NiAl-LDH. It was proposed that at low pH, the large number of positive charged binding sites on the NiAl-LDH (due to protonation) electrically attract the anionic MO and with increased pH electrical repulsion sets in thereby reducing adsorption.

2.5.2 Contact Time

Contact time is a significant parameter to consider in the interaction between contaminants/ pollutants and adsorbents. In general, adsorption increases with contact time until equilibrium is attained. The equilibrium time greatly depends on the factors such as composition/ type of LDH, the precursors used for the synthesis, the adsorbent dosage and initial dye concentration. According to Ahmed and Gasser [50], an approximate equilibrium time of 15 minutes is needed for removal of about 98 % of Congo Red by MgFe–CO_3 using 0.003 g/mL adsorbent dosage in a 100 mg/L Congo Red solution

Equilibrium times of 20 and 140 minutes were reported for initial dye concentrations of 20– 80 mg/L and 120–160 mg/L respectively indicating an increase in equilibrium time with increased initial dye concentration[41].

2.5.3 Initial Solution Concentration

This effect varies from one LDH to the other. It was reported that the adsorption at equilibrium increased from 8 to 65 m/g for an increase in initial dye concentration from 20 to 160 mg/L[41]. For the case on Methylene orange adsorption on ZnMgAl-LDH, degree of removal of the dye reduces on increasing the initial dye concentration from 0.07 to 0.12 g/L [37]. This was due to reduction in active sites for MO adsorption

2.5.4 Adsorbent Dosage

The amount of adsorbate removed (removal efficiency) from an aqueous solution generally increases with adsorbent dosage [51]. From the study of Shan and his group[33], the removal of the adsorbates (the 3 red dyes) increased with increase in adsorbent dosage until an equilibrium is attained. Though the removal efficiency for methylene orange increased with increase in adsorbent dosage but it was reported that a decrease in adsorption capacity reduced (from about 520 to 44.32 mg/g) with increasing adsorbent dosage (2.5 to 30mg) by biomorphic MgAl-LDH [52]. The increase in removal efficiency of the dye was attributed to increase in number of adsorption sites [49].

2.5.5 Thermodynamic Study and Temperature

Thermodynamic parameters are indicators of spontaneity and feasibility of adsorption processes. The significance of temperature on adsorption is studied through change in standard free energy (ΔG), change in entropy (ΔS) and change in enthalpy (ΔH) which are

extracted from experimental data at various temperature using the following relations [50]

$$\Delta G = -RT\ lnK_D \qquad 2.1$$

$$lnK_D = \frac{\Delta S}{R} - \frac{\Delta H}{RT} \qquad 2.2$$

K_D defines distribution coefficient, T is absolute temperature and R is molar gas constant. ΔH and ΔS relationships with ΔG is expressed are expressed according to the following equations [43].

$$\Delta H = -R(\frac{T_2T_1}{T_2-T_1})ln\frac{K_1}{K_2} \qquad 2.3$$

$$\Delta S = \frac{\Delta H-\Delta G}{T} \qquad 2.4$$

K_2 and K_1 are the Langmuir constants T_2 at and T_1 respectively. A positive ΔH indicates endothermic reaction while negative value denotes exothermic process. A positive ΔS indicates increased randomness of adsorption process. A negative ΔG depicts the spontaneity of the process [41].

The influence of temperature is determined nature of heat change involved on the adsorption process which can either be endothermic or exothermic. For an endothermic adsorption system, the amount of adsorbate removed by the adsorbent increases with increasing temperature as was observed in methyl orange (MO) adsorption by calcined NiAl-LDH [43]. The converse happens for exothermic adsorption system which involves decrease in adsorption by adsorbent with increasing temperature.

2.5.6 Coexisting ions

Several articles have been published showing influence of coexisting ions on adsorption by LDHs and also its composites [45, 53-55]. The coexisting ions may improve adsorption of the specie of concern on the LDH. This case was reported for Methylene blue (a cationic dyes) removal from aqueous solution in the presence of anionic components with higher removal capacity ($HPO_4^{2-} > SO_4^{2-} > Cl^-$) [45]. The converse of inhibiting adsorption occurs for the case of competing ions. For As(V) adsorption on LDHs, interference of competing ions follows the order $HCO_3^- > HPO_4^{2-} > SO_4^{2-} > Cl^-$ while that of As(III) follows $HPO_4^{2-} > SO_4^{2-} > CO_3^- > F^- > Cl^- > Br^- > NO_3^-$ [15]. In industrial application, wastewater contains coexisting ions which will always compete for adsorption sites. CO_3^{2-}, SO_4^{2-}, $H_2PO_4^-$ and Cl^- will always strongly compete with Cr(VI). 85.0%, 75.0%, 24.2%, and 13.3% reduction in adsorption of was recorded on Cr(VI) was recorded in the presence of 20 mmol/L of CO_3^{2-}, SO_4^{2-}, $H_2PO_4^-$ and Cl^- respectively [10]

2.6 Adsorption Isotherm

Adsorption isotherm is an indication of extent of distribution of adsorbate between the solid phase and liquid phase upon reaching equilibrium in the adsorption process. Two of the well-established isotherms are the Langmuir and Freundlich isotherms. Among other isotherms belongs the Sips [56], Temkin [57], Redlich–Peterson [43], Dubinin–Radushkevich [58] .The Langmuir isotherm which is based on monolayer adsorption assumes homogeneous adsorption sites possess with equal energy [59] and non-linear form is given by

$$q_e = \frac{q_m\, b\, C_e}{1 + b\, C_e} \qquad 2.5$$

In linear form, equation 2.3 is expressed as

$$\frac{C_e}{q_e} = \frac{1}{b\, q_m} + \frac{C_e}{q_m} \qquad 2.6$$

Where q_e is quantity of dye adsorbed (mg/g), C_e is amount of dye adsorbed at equilibrium (mg/L) and the langmuir contants q_m (mg/g) and b (L/mg) are the maximum monolayer adsorption of the adsorbent and relation to free energy of adsorption respectively[41]. A consolidating parameter to determine the favourability or non-favourability of the adsorption system is the essential factor (or equilibrium parameter or separation factor), R_L defined by Chen et al.[60] as

$$R_L = \frac{1}{1 + b\, C_0} \qquad 2.7$$

Where $R_L > 1$, $R_L = 1$, $0 < R_L < 1$ and $R_L = 0$ indicate unfavourable, linear, favourable, and irreversible adsorption. C_0 is the highest initial dye concentration (mg/L)

Freundlich isotherm, which is appropriate for low concentration, assumes a heterogeneous surface with heat of adsorption distribution [43] and mathematically represented as

$$q_e = K_F\, C_e^{1/n} \qquad 2.8$$

Equation 2.6 can also be converted to linear form as given in equation 2.7

$$\log q_e = \log K_F + \frac{1}{n} \log C_e \qquad 2.9$$

C_e and q_e retains the same definition as previously defined. n and K_f are Freundlich constants in which n indicates the extent of nonlinearity between adsorption and

concentration of solution and provides information on favourability of adsorption while K_f ($mg^{1-1/n} L^{1/n} g^{-1}$) shows degree of adsorption.

Redlich-Peterson (RP) isotherm is a 3-parameter model that combines Langmuir and Freundlich isotherms [61]. The relation approaches Langmuir isotherm at low concentration and Langmuir at high concentration. RP isotherm is defined as

$$q = \frac{A\,p}{(1+ B\,p^{g})} \qquad 2.10$$

Temkin isotherm [62] considers the adsorbate- adsorbent interaction where the heat adsorption reduces linearly with coverage for all molecules. In nonlinear and linear forms it is represented respectively as

$$q_e = B \ln(A\,C_e) \qquad 2.11a$$

$$q_e = B\,lnA + B \ln C_e \qquad 2.11b$$

and B is defined by

$$B = RT/b_T \qquad 2.12$$

1/ b_T defines the adsorbent adsorption potential T and R stands as previously defined. In the qe versus Ce, there will be a linear reduction in energy of adsorption as adsorption sites are occupied. There is linear decrease in heat of adsorption with surface coverage because of adsorbate-adsorbent interaction. There is also an assumption that there is homogeneous distribution of binding energy to peak during the adsorption.

2.7 Adsorption Kinetics

Pseudo-first order and pseudo-second order are the prominent models used to predict sorption process mechanism[63]. The pseudo-first order model (named as Lagergren's pseudo-first-order model) which considers diffusion through a boundary layer prior before adsorption is given as

$$log(q_e - q_t) = \ logq_e - \frac{k_1\, t}{2.303} \qquad 2.13$$

Where q_t is time-dependent amount of dye adsorbed per unit of adsorbent (mg/g) during time contact time t (min), k_1 is the pseudo-first order rate constant (min^{-1}). k_1 is obtained from the plot of log ($q_e - q_t$) versus t. The pseudo-second order model is as follows k_2 is the pseudo-second order rate constant (g mg^{-1} min^{-1}).

$$\frac{t}{q_t} = \ \frac{1}{k_2\, q_e^2} + \frac{t}{q_e} \qquad 2.14$$

One of the parameters to determine which model to choose is the statistical tool correlation co-efficient (R^2). The high R^2 shows strong correlation between the model and experimental data, hence the model with the highest R^2 will be considered as the appropriate model to depict the experimental data. In most of the studies a $R^2 > 0.97$ provides high confidence in the model considered.

2.8 Impact of Calcination and Adsorption Temperature

Calcination affects the structure, texture and performance of LDHs. The thermogravimetric analysis (TGA) of Ni-Al LDH shows three regions of weight loss [43]. The first (below 230^0C) is associated with loss of physisorbed as well as interlayer H_2O molecules [64]. The second region (between 230^0C and 500^0C) indicates removal of NO_2 and OH from the

interlayer anions and brucite structure respectively. Beyond the region 2 (above 500^0C), no further weight loss and phase change was observed. This was further corroborated by DTG which shows total breakdown of the LDH at 345^0C. The resultant specie is a mixed metal oxide (MMO)

In the work Zhi-qing Zhang et al.[29], he reported the XRD analysis that the characteristic reflection of LDHs at (003), (006) and (009) becomes weak and increased production of reflection at (200) and (300) associated with MgO as calcination temperature is increased. These observed weak reflections at 300^0C and 400^0C imply the layered are maintained but there is a resultant dehydration and dehydroxylation [65]. At higher temperatures (500^0C and above), the reflections associated with LDH disappeared and those associated with typical mixed metal oxide (MgO) becomes visible.

In the same work of Zhi-qing Zhang et al.[29], the group showed that at the 300^0C calcination temperature, the peak at 1630 cm^{-1} was visibly absent as a result of elimination of interlayer water molecules. Also the reduction of peak intensities at t 1054, 1384 and 1560 cm^{-1} from 300^0C to 400^0C was due to continuous elimination of $CO3_2^-$ and peak associated with $CO3_2^-$ completely vanished for calcination temperature of 500^0C implying a complete destruction of the hydrotalcite configuration. It becomes interesting to note an impure $MgAl_2O_4$ phase is formed upon calcination at 600^0C.

According to SEM analysis in the work of Zhi-qing Zhang et al.[29], calcination temperature greatly affected the textural properties of the LDHs. The pore volume (PV) and specific surface area (SSA) increase with temperature (a maximum of 500^0C) after which a decline of these properties occurs at 600^0C due to for formation of impure phase

MMO (agglomeration and sintering occurrence). The pore size was not significantly affected by calcination.

2.9 Regeneration and Recovery of LDHs

Regenerating LDHs adsorbents is one of the key economic parameters to be considered in the industrial feasibility of the use of LDH. Various studies have been performed on the regeneration mode using reagents such as sodium carbonate, mineral acids, ammonia solution, mineral acids as well as combustion. Organics-laden LDHs can be combusted at relatively high temperature to completely remove the adsorbates [66]. Ahmed and Gasser [50] combusted Mg–Fe–Dye–LDH for 2 hours to completely alienate Congo red from the adsorbate. Carbonate and chloride solutions could help regenerate oxyanion-ladened LDHs [15]. Bacteria culture have been used to regenerate Methylene blue loaded LDH and this improved the adsorption capacity of the LDH on the first regeneration cycle through synergistic effects [45]. Acetone extraction along with drying was used in the recovery ZnAl–$PW_{10}Mo_2$ LDH after it adsorption of Methylene blue [24]. It is worthy of note to report that second adsorption cycle yielded a poor 33% which may be of economic viability though it was indicated that the poor result may be due to partial extraction of the adsorbate from the adsorbent.

After several cycles of regeneration of LDHs, the adsorption capacity of the LDH will reduce and this may be due to reduction in crystallinity of the LDH [67], thus affecting it continuous use for adsorption purpose.

Recovery of LDH from water in industrial process is an arduous task, Yan et al.[68] synthesised a Fe_3O_4 / LDH nanocomposite as a magnetic adsorbent of Ur(IV) ions from

water. This enables easy separation of the composite by a magnet after the adsorption process.

CHAPTER 3

EXPERIMENTAL AND METHODOLOGY

3.1 Synthesis of LDHs and its Nano-Composites

The LDHs samples were all prepared by coprecipitation method. To prepare the nano-composite, ultrasonication was applied to ensure effective dispersion.

3.1.1 Materials and Reagents

The following are the reagents used without further purification:

1. Nitrate salts: $Co(NO_3)_2 \cdot 6H_2O$, $Ni(NO_3)_2 \cdot 6H_2O$, $Mg(NO_3)_2 \cdot 6H_2O$, and $Al(NO_3)_3 \cdot 9H_2O$ (all purchased from Sigma-Aldrich)
2. NaOH (from Panreac AppliChem, Darmstadt, Germany)
3. Acids: HCl (from Eurostar, Liverpool UK) and HNO_3
4. Hydrazine
5. Ethanol
6. Graphene (GRAFEN®-SEG / Semi-exfoliated Graphene Sheets): diameter ~200 µm, thickness < 50 nm
7. Deionized water

3.1.2 Synthesis of Ternary LDHs and Graphene/ Ternary LDHs nanocomposites

The procedure was followed from the work of Zubair et al. [32] with slight adjustment. The preparation of NiMgAl LDH (NMA) is shortly described as follows. 0.02 mole of $Al(NO_3)_3 \cdot 9H_2O$, 0.02 mole of $Ni(NO_3)_2 \cdot 6H_2O$ and 0.04 mole of $Mg(NO_3)_2 \cdot 6H_2O$ (total ratio

of M^{2+} to M^{3+} is 3) were dissolved in 60 ml of deionized water in a 500-ml round bottom flask. The was stirred vigorously at 600 rpm in an oil bath at 60^0C for 15 mins. Subsequently 1M NaOH was added dropwisely to stabilize the pH at 10 ± 0.5 while maintaining the stirrer speed and temperature of 60^0C. Thereafter, the temperature was raised to 90^0C and stirring increased to 900 rpm while the reaction was refluxed for 24h. The suspension obtained was subjected to centrifugation and washed twice with deionized water and then followed by twice washing using ethanol to remove impurities. The densely-obtained slurry was dried in a vacuum oven at 90^0C for 24-48h. In the synthesis of MgCoAl LDH (MCA), the same procedure outlined for NMA synthesis was followed with Ni substituted by Co and the molar ratio was maintained (Mg: Co: Al = 2: 1: 1)

As for graphene/ ternary LDHs nanocomposites, 300 mg of graphene was added to 60ml NaOH (0.2 M) and the mixture ultrasonicated at 60 rpm for 90 min. The obtained mixture was then added to a prepared mixture of the ternary LDHs precursor and two to three drops of hydrazine was added as a complexing agent. Other procedures were followed as outlined in the synthesis of NMA. Both ternary NMA and G/NMA were calcined at 400^0C for 3h under 120 mL min^{-1} N_2 environment to produce NMA-C and G/NMA-C respectively and stored for use in adsorption experiment. Likewise, MCA and G/MCA was subjected to calcination in similar manner to generate MCA-C and G/MCA-C respectively.

3.2 Characterization Techniques

For excellent description of the as-synthesized samples, characterizing the LDHs and its nanocomposite samples was done by: (i) Scanning Electron Microscope Analysis (ii) X-Ray diffraction (XRD) (iii) FTIR spectroscopy and (iv) Thermogravimetry analysis. These are briefly explained below

3.2.1 XRD Analysis

XRD is resourceful, non-destructive technique which shows comprehensive facts about the crystallographic and micro structure of all kinds of natural and synthetic materials. This method is applied in different sectors of life. In order to detect the crystallographic structure of catalyst samples, patterns of diffraction are employed. One essential drawback of this techniques is that non-crystalline phase(s) and minute particle(s) can give wide and feeble lines of diffraction and in some instances will give no line of diffraction. This occurrence will eventually make them practically undetectable to X-Ray Diffraction.

Powder X-Ray Diffraction (XRD) measurements will be considered to detect the crystallographic structure of the synthesized LDHs and its nanocomposite samples. The XRD diffraction patterns of the catalyst samples will be gotten by utilizing an MinifeFlex II instrument from Rigaku Instruments with a monochromatic Cu Kα radiation source (wavelength = 0.15406 nm, 30 kV, 40 mA) and a normal scan rate of 3 scans per minute within the 2θ range of 5-70 degrees with a step size of 0.03

3.2.2 Scanning Electron Microscope Characterization

The scanning electron microscope is a tool used for material characterization with the aim of obtaining information about the structure, composition and defects in materials. The images are obtained by scanning electron beam of high energy on the sample surface. The scanning electron provide information about surface topography, shape, size and structure of grains, failure analysis, and elemental distribution. It uses a spatial resolution of 1 nm and sampling depth of 1-5μm. It can be used to analyze sample of area of <1 to 100 μm. It has detection limits of 0.2 wt%. It is generally applied for solid samples.

Each of the samples will be analyzed by the SEM while ensuring that the microscope is aligned to avoid lack of sharpness and focus. Other necessary precautions is to ensure large objective aperture in order to have low resolution, small depth of field, small smooth image and make it suited to micro-chemical analysis. An electron beam is incident across each catalyst sample resulting in the generation of secondary and back scattered electrons which are used to form images and X rays are used to obtain elemental constitution of the catalyst samples. This characterization will reveal the structure and elemental composition of all the five catalyst samples.

3.3 Adsorption Experiment

The adsorption experimental process was carried out to investigate and select the optimum process parameters need LDHs removal of anionic dyes. These are pH, adsorbent dosage, concentration of dye, temperature and contact time. From the data obtained, information on the appropriate kinetics, isotherm as well mechanism behind the adsorption process can be presented.

The percentage dye removal (%), time-dependent adsorption capacity (q_t) and equilibrium adsorption capacity (q_e) and are computed from the following equations

$$\%\ Dye\ removal = \frac{C_o - C_e}{C_o} * 100 \qquad 3.1$$

$$q_t = \frac{C_o - C_t}{M} * V_S \qquad 3.2$$

$$q_e = \frac{C_o - C_e}{M} * V_S \qquad 3.3$$

Where C_o, C_e, C_t,V_S and M respectively represent initial concentration of dye solution (mg/L), equilibrium concentration of dye solution (mg/L), concentration of dye solution (mg/L) at time t, volume of dye solution used (mL) and weight of adsorbents (mg).

3.3.1 Determination of Optimum pH

30ml of 30 ppm dye solution was placed in each seven 100 ml conical flask. The pH adjustment from 2 to7 of each flask solution was carried with 0.1M HCl or 0.1M Na0H. 10 mg of as-prepared LDHs samples was subsequently added to the solution. These flasks were then put on a shaker and operated at 180 rpm for 24 h to enable establishment of equilibrium. Thereafter, the sample were centrifuged to obtain the supernatant and the solid residue. The supernatant was analysed using UV-Visible spectrometer under the area of maximum absorbance to determine the concentration of dye remaining.

3.3.2 Determination of Adsorbent Dosage Effect

Upon determining the optimum pH needed to maximize adsorption, the influence of dosage of adsorbent is considered in the experiment. This is done by preparing a given concentration such as 30 ppm of dye solution in a 100ml conical flask and adjusting at the optimum pH using either 0.1M HCl or 0.1M Na0H. Different dosage of adsorbent: 5mg, 10mg, 15mg, 25mg, 40mg, 55mg and 70mg will be added to each flask and the flasks place on the shaker operated at 250 rpm for 24h to ensure equilibrium adsorption. The obtain samples are centrifuged and subsequently analysed for absorbance using UV-Visible spectrometer. The obtained data of absorbance versus dosage is tabulated, plotted and analysed to determine optimum dosage for the given concentration of dye solution

3.3.3 Determination of Effect of Dye Concentration

This will be carried out at temperature of 25^0C. 20-160 ppm of dye concentration will be prepared in 100ml conical flask and the pH adjusted to the optimal value. 10mg of the as-synthesized LDHs adsorbent will be added to each flask and the flask agitated on the shaker at 250 rpm for 24 h. The obtained samples are then centrifuged and the absorbance obtained. The obtained data is tabulated, plotted and analyse to determine the significance of dye concentration on the adsorption process.

3.3.4 Determination of Effect of Contact Time

The dye removal efficiency expressed in terms of absorbance is being plotted at different concentration (20, 40 and 100 ppm) as a function of contact time (0-24 h). The procedure follows what has been previously outlined in 3.3.1 to 3.3.3 but additionally, the samples are prepared an analysed for absorbance at different contact time such as 5min, 10min, 15min, and so on until for 24 hrs.

CHAPTER 4

Graphene/ Ternary Layered Double Hydroxide

Nanocomposites For Efficient Adsorption Of Eriochrome Black T

From The Aqueous Phase

This chapter reports the result of sorption of Eriochrome Black T (EBT) from aqueous phase using ternary LDH and its nanocomposites. For simplicity of understanding uncalcined NiMgAl, calcined NiMgAl, uncalcined graphene-NiMgAl and calcined Graphene-NiMgAl are referred to as NMA, NMA-C, G/NMA and G/NMA-C respectively

4.1 Characterization of NMA, G/NMA, NMA-C and G/NMA-C

XRD patterns of the NMA, G/NMA, NMA-C, and G/NMA are displayed in Fig 4.1. Both the NMA and G/NMA LDHs exhibited high reflection peaks at 10.96°, 22.08° and 34.77° with interplanar spacing of 8.06 A, 4.02 A and 2.58A and corresponding to 003, 006, and 009 planes respectively. The peaks at 38.75°, 45.7° ,60.89° and 61.42° are assigned to 015, 018, 110 and 113 planes respectively [69]. The result indicates the as-synthesized LDHs possess high crystallinity with well layered structure. Additional peaks at 26.46° corresponds to 002 plane [70] due graphene crystallinity was found in the G/NMA which indicates good integration of the graphene into the LDHs structure and this may inherently improve its adsorption performance. Calcination led to the elimination of physisorbed and interlayer H_2O molecules, and interlayer anions with a resultant collapse of LDHs lamellar

structure. The result for the NMA-C and G/NMA-C shows the destruction of the LDHs structure after calcination with a resulting formation of mixed metal oxides MgO/NiO. Due to the relatively low temperature of calcination, no peaks assigned to any aluminium oxide specie such as spinel ($MgAl_20_4$) which crystallizes at high temperature and it indicates dispersion of Al^{3+} into the solid matrix solution of MgO [71-73]

Fig 4.2 depicts the characteristic FTIR spectra of a typical LDH. The broad between 3300-3800 cm^{-1} is associated with the stretching vibrations of OH group of interlayer H_2O in the brucite- like layers [32]. This band becomes attenuated upon the calcination of the hydrotalcite. The weak band at 1640 cm^{-1} corresponds to bending vibrations of OH of water molecules. The strong band at 1350cm^{-1} LDH which shift to weak band at 1390cm^{-1} indicates antisymmetric vibrations associated with Nitrate ions. Though this band attenuated, it was not completely removed indicating removal of the interlayer anion and a collapse of the LDH as (confirmed from XRD patterns). Peaks associated with carbonate are located around 1000-1100 cm^{-1} (bending non-polar mode), 800-900 cm^{-1} (torsion mode), 600-700 cm^{-1} (bending angular mode) [33]. The M-O, M-O-M and O-M-O peaks are found below 1000 cm^{-1}.

Fig 4.3 shows the microstructure of the asynthesized NMA, G/NMA, NMA-C, and G/NMA. The NMA comprises of small particles which aggregate to form platelet morphology. Addition of graphene to LDH resulted in overlapping nanosheets in G/NMA Upon calcination, rough, compact and homogeneous surfaces comprising of nanoparticle formed. The calcined samples display larger pores which can facilitate the adsorption process.

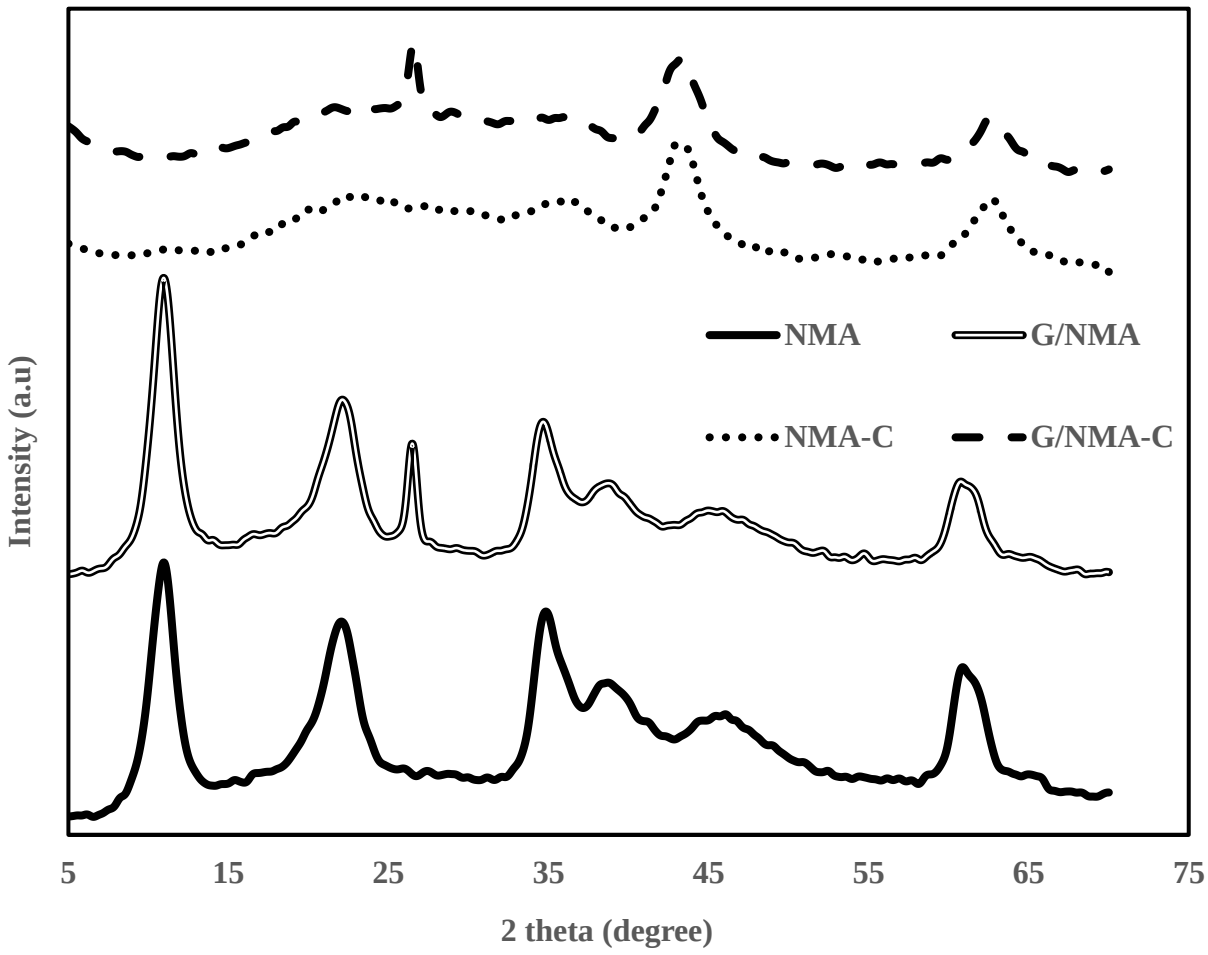

Fig 4.1 XRD of NMA, G/NMA, NMA-C, and G/NMA-C.

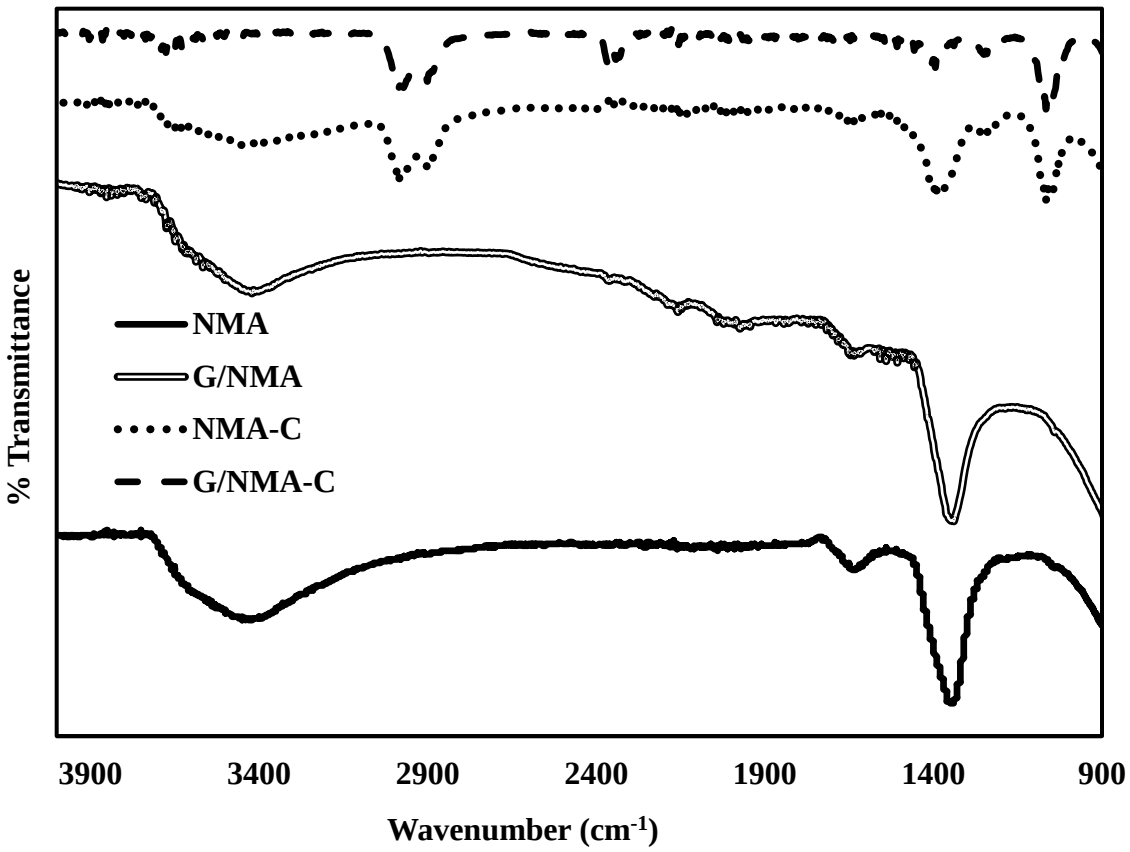

Fig 4.2 FTIR spectra of NMA, G/NMA, NMA-C, and G/NMA-C.

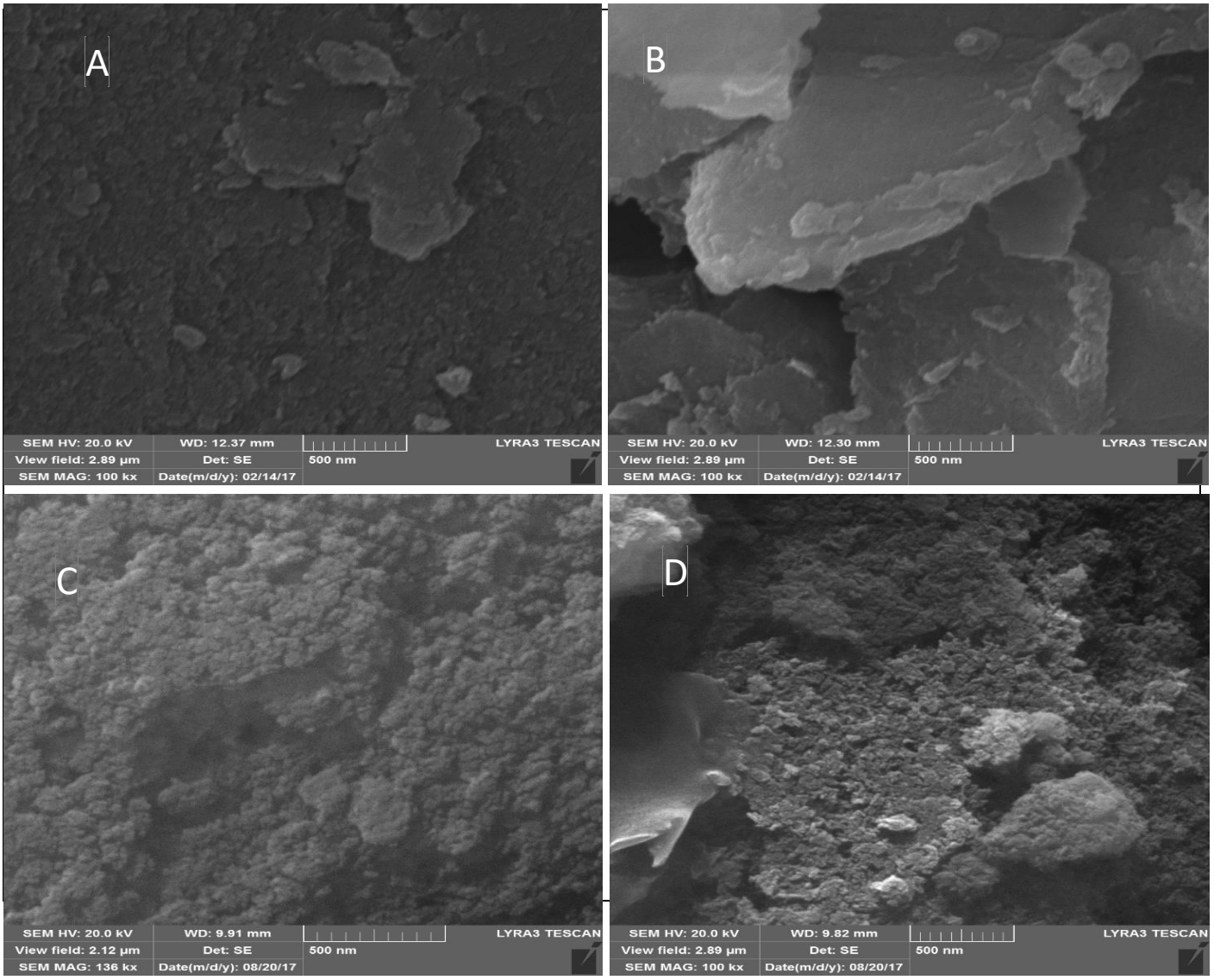

Fig 4.3 SEM of (A) NMA (B) G/NMA (C) NMA-C and (D) G/NMA-C.

Fig 4.4 depicts the thermogravimetric analysis (TGA) which shows the decomposition pattern and thermal stability of the LDHs and its graphene hybrid. Three stages of weight loss occur under the thermal treatment up to temperature of 800°C. Physisorbed and intercalated water molecules are removed up to a temperature of 170°C with a resultant weight loss of 11.5% and 10.5% for NMA and G/NMA respectively. At the second stage, 23.5% for NMA and 22% for G/NMA in weight loss occur between 170°C and 370°C. This was due to decarbonation, dehydroxylation and elimination of other interlayer anions [74].The second weight loss resulted into formation of mixed metal oxides (MMO). Thermal treatment above 370°C with little weight loss led to continuous decarbonation and decarboxylation and more formation of MMO. The total weight loss upon thermal exposure suggest good thermal stability of the synthesized material with G/NMA possessing better higher stability

4.2 Adsorption Parameters

Effects of parameters such as pH, contact time, adsorbent dosage, EBT concentration and temperature were studied

4.2.1 Effect of Initial pH

The surface charge as well as degree of ionization of adsorbate of the adsorbent is a major effect of pH which controls adsorption processes [41, 45]. The influence of pH (range of 2 to 8) on removal of EBT was carried using 0.01g of adsorbate in 30ml of 40mg/L dye solution operated at 180 rpm and 25°C for 8hrs. The result of Fig 4.5 shows that removal reduces as pH increase until 4 after which the removal efficiency decreases except for calcined G-LDH which maintains a relatively constant percentage removal at higher pH

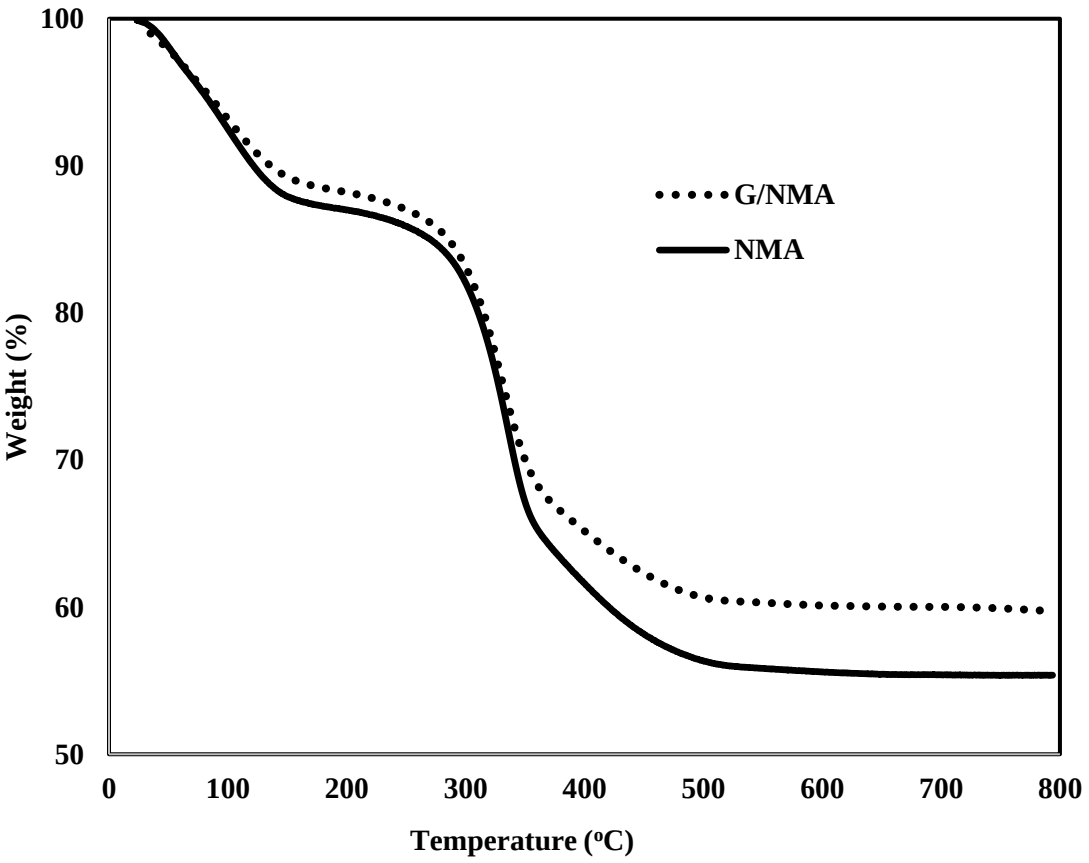

Fig 4.4 TGA of NMA and G/NMA

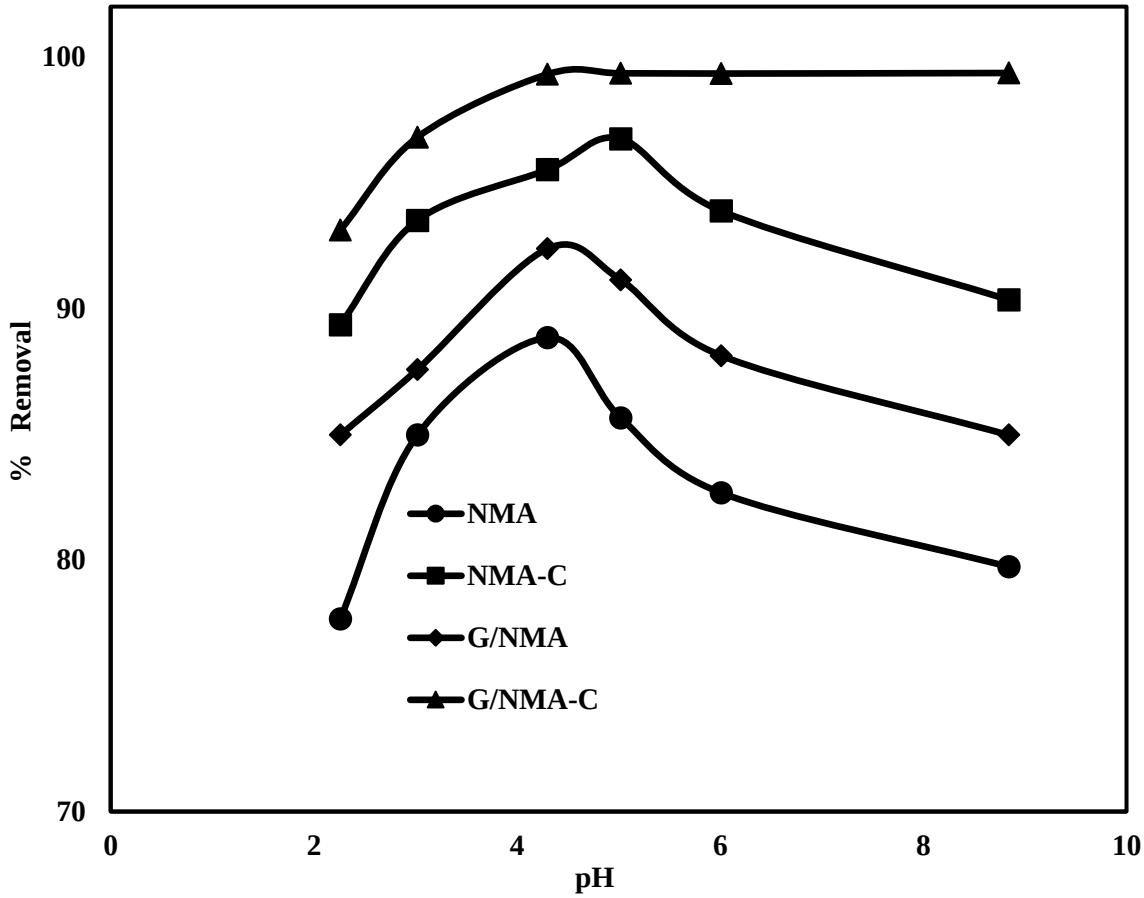

Fig 4.5 Effect of pH on percentage removal of EBT

values. This can be a significant advantage in the practical use of calcined G-LDH in dyes removal due to its pH independence when compared to other adsorbents which performances significantly depend on pH adjustment. The maximum percentage removal recorded for NMA, G/NMA, NMA-C and G/NMA-C are 88.8, 92.3, 96.5 and 99.3 % respectively. The higher dye removal experienced by graphene hybrids were due to increased surface area contribution of the graphene. At very low pH, the structure of the layered material becomes impaired resulting in instability and leads to dissolution of the adsorbate and this reduces the adsorption performance of the adsorbates [75-77]. At higher pH values, increasing competition of OH^- for adsorption sites reduces removal of the anionic dye [69].The optimum pH for the adsorption study was 4 and this was used for the rest of the experiment.

4.2.2 Effect of Contact Time

Fig 4.6 shows the influence contact plays on percentage removal of EBT for time range of 0 to 480 min. The percentage removal rises with increase in the contact time with rapid sorption in the first 15 minutes. This is an indication of strong polarity of the LDH surface to rapidly attract high number of dye molecule enhanced by large surface area [78]. Thereafter the rate gradually reduced until equilibrium was established at 240, 180, 90 and 60 min for fresh samples of NMA, NMA-C, G/NMA and G/NMA-C respectively. The faster adsorption rate of the graphene hybrid compared to the non-hybrid may be due to higher surface area. The higher adsorption rate of calcined sample when compared to uncalcined sample can be attributed to memory effect [15, 79]. The highest adsorption rate demonstrated by G/NMA-C shows synergistic interaction of graphene hybridization and calcination [79].

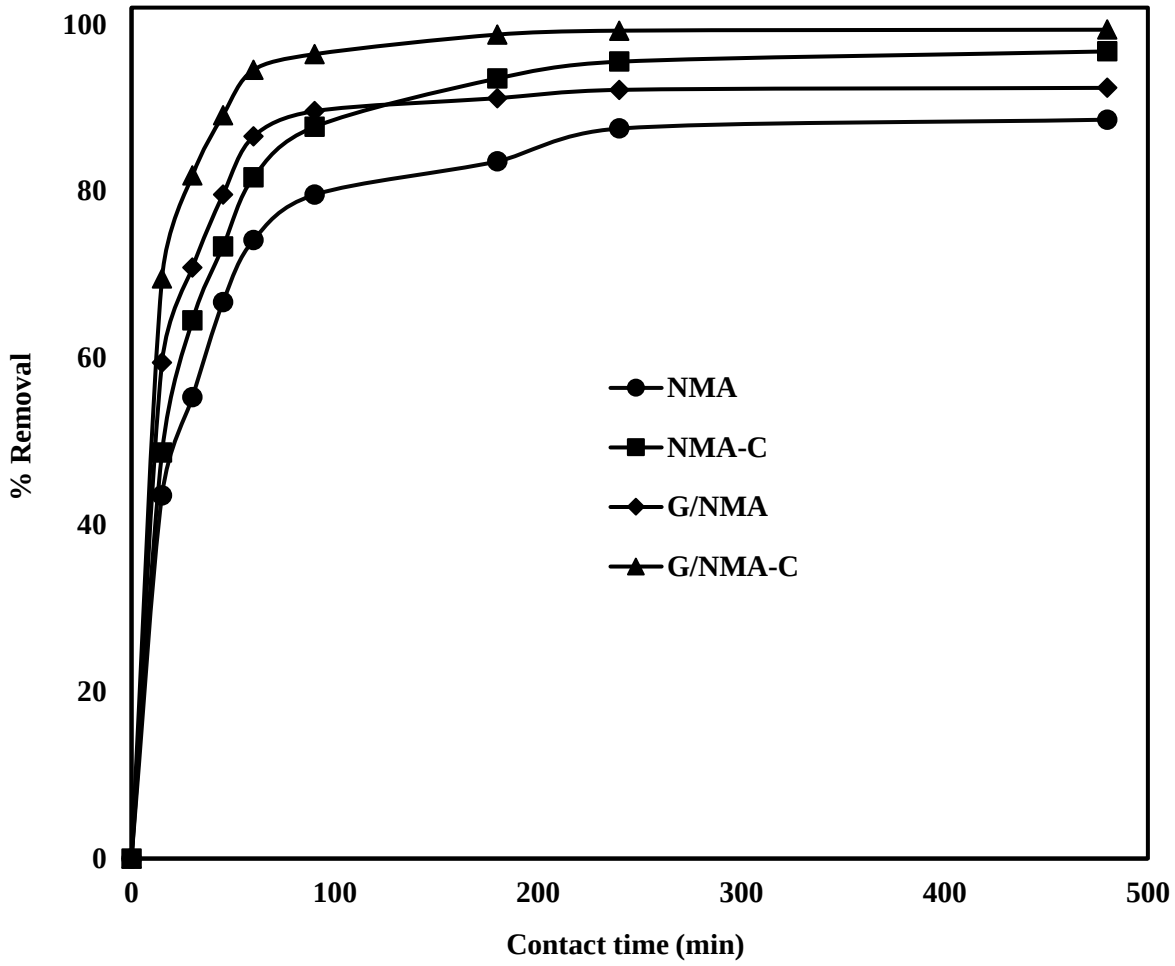

Fig 4.6 Effect of contact time on percentage removal of EBT. Adsorbent dosage 10mg; C_0 = 40 mgL^{-1}

4.2.3 Effect of Dosages

Fig 4.7 displays the effect of adsorbents NMA, G/NMA, NMA-C and G/NMA-C dosages on adsorption of EBT. From the plot, two stages of adsorption are established. The first stage shows increase in EBT removal with a rise in adsorbent dosage. This is related with increase in active adsorption sites with increased supply of adsorbent. The second stage involves occurrence of a plateau signifying no further increase in adsorption with increased dosage. This indicated that the number of adsorption sites more than satiates the available number of dye molecules. As shown, the calcined samples recorded higher adsorption performance with increased dosage when compared to its uncalcined counterpart. Likewise, the hybrid shows better performance than the nonhybrid which may be associated to increased surface area. An increase of adsorbent dosage from 2mg to 10mg resulted in percentage increase of EBT adsorption from 6, 23, 11 and 36% to 87, 91, 96, and 99 % for NMA, G/NMA, NMA-C and G/NMA-C respectively. Except for calcined G-LDH whose percentage removal plateaus at 10mg, G/NMA show increased adsorption with adsorbent dosage while both NMA and NMA-C establish a plateau at 15mg for removal of 92 and 99% EBT respectively. This shows superior advantage of calcined G-LDH which possesses synergistic properties of hybridization and calcination. For subsequent experimental study, 10 mg of adsorbent was used.

4.2.4 Effect of Initial EBT Concentration

Fig 4.8 shows the effect of initial EBT concentration on percentage removal of dye. As the initial concentration of dye increases, the percentage removal reduces. Since adsorbent dosage is fixed, the number of adsorption sites are fully satiated with dyes molecules

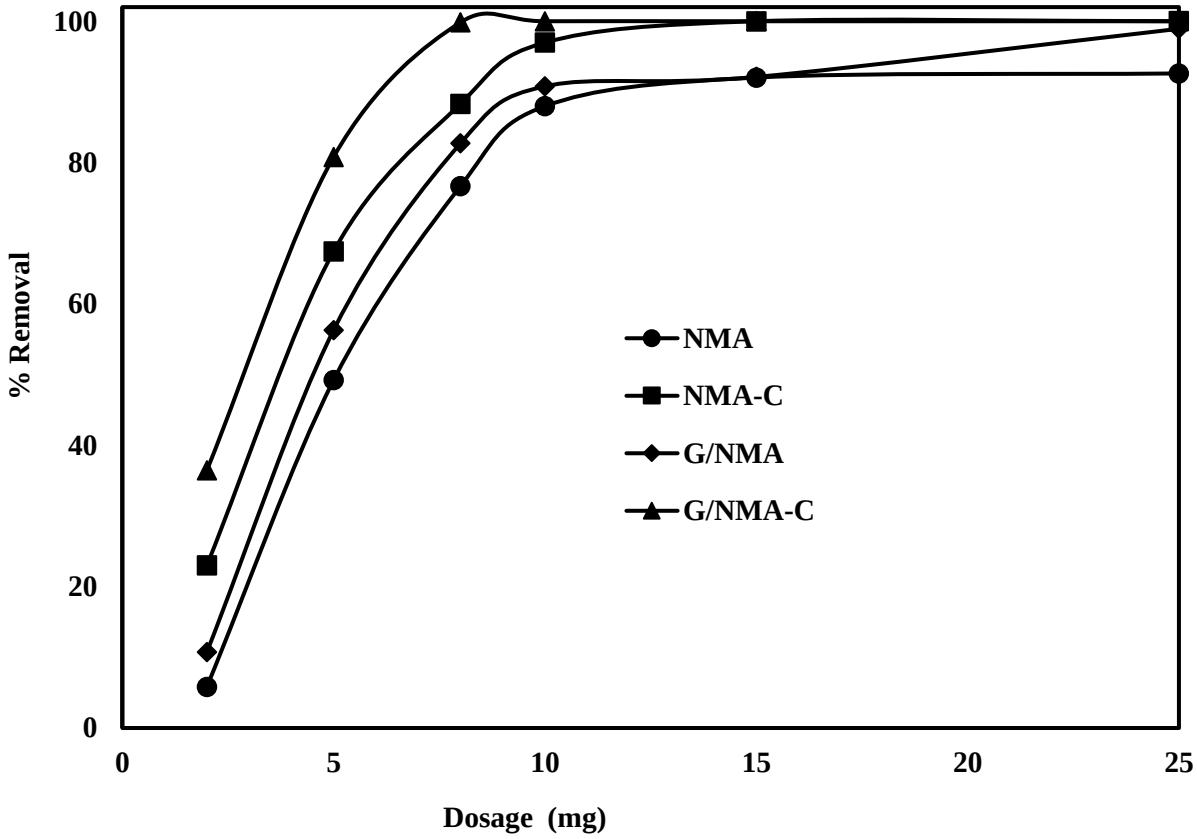

Fig 4.7 Effect of Dosage on percentage removal of EBT. Contact time= 180mins; C_0 = 40 mgL^{-1}

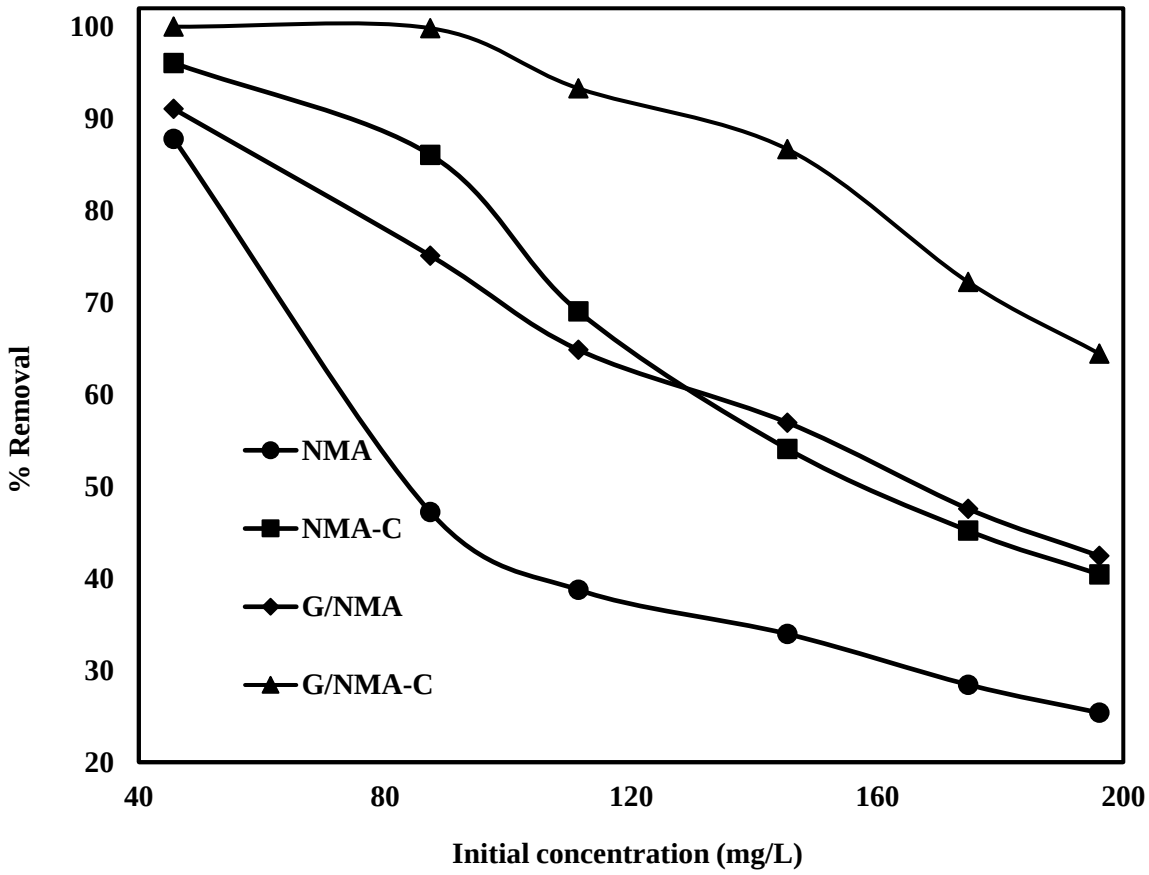

Fig 4.8 Effect of concentration on percentage removal of EBT. Contact time= 180mins; Adsorbent dosage= 10 mg

rendering more dye molecules unadsorbed as the initial dye concentration is increased. This thus translates to a reduction on percentage removal with increase in initial dye concentration [69]. The percentage removal of EBT decreased from 87.8, 91.1, 96.1, and 99.9 % to 34.0, 64.9, 69.0 and 93.3% for NMA, G/NMA, NMA-C and calcined G/NMA-C respectively for change in concentration from 45 mg/L to 110 mg/L. The result further confirms that the graphene with LDH resulted in higher performance in adsorbing EBT. The surface of composites as confirmed from FTIR and XRD results improved the interaction of composite with EBT

4.3 Isotherm Studies

Adsorption isotherm is an indication of extent of distribution of adsorbate between the liquid phase and solid phases upon reaching equilibrium in the adsorption process [43]. In this study, three different temperatures and two well-established isotherm models, Langmuir isotherm and Freundlich isotherm, are considered.

The experimental data are fitted to the linear forms of Langmuir isotherm model (equation 2.6) and Freundlich isotherm model (equation 2.9) and the parameters obtained are shown is Table 4.1. The Langmuir isotherm with correlation coefficient > 0.98 fits the experimental data in comparison to Freundlich isotherms for all the adsorbents and temperature under consideration. The maximum adsorption capacity computed at 25^0C from the Langmuir model are 156.25, 263.16, 238.14 and 384.62 mg/g for NMA, G/NMA, NMA-C and calcined G/NMA-C respectively. The value of $1/n < 1$ found in table 1 further buttress the suitability of Langmuir isotherm in describing the adsorption process [80]. This is indicative of a homogeneous surface accompanied by monolayer adsorption. The value of $R_L < 1$ for all the sample shows that the adsorption is favorable.

Table 4.1 Parameters of Isotherm models for adsorption of EBT

Sample	T (K)	Langmuir			Freundlich		
		Q_m (mg/g)	R_L	R^2	K_F	1/n	R^2
NMA	298	156.25	0.0350	0.9922	104.1838	0.0666	0.6998
	308	136.97	0.0265	0.9974	98.3105	0.0572	0.9677
	323	126.97	0.0307	0.9991	84.1589	0.0712	0.9941
G/NMA	298	263.16	0.0310	0.9922	95.8959	0.2165	0.8661
	308	256.41	0.0678	0.9794	94.0156	0.1798	0.9530
	323	217.39	0.0673	0.9921	90.3026	0.1595	0.9707
NMA-C	298	238.1	0.0220	0.9933	146.7912	0.1146	0.9643
	308	204.23	0.0190	0.9842	122.5180	0.0971	0.9911
	323	188.68	0.0176	0.9882	107.1026	0.1113	0.9687
G/NMA-C	298	384.62	0.0020	0.9955	283.7919	0.0762	0.9830
	308	370.37	0.0180	0.9977	248.4277	0.0802	0.9749
	323	322.58	0.0241	0.9974	227.2480	0.0697	0.9734

4.4 Kinetic Studies

To predict feasible sorption process mechanism, adsorption rates were investigated using both pseudo-first order and pseudo-second kinetic models [63]. The kinetic data are fitted to the linear forms of the pseudo-first order (equation 2.13) and pseudo-second order (equation 2.14) modelsThe kinetic parameters calculated from the linear regression and the correlation coefficients are summarized in Table 4.2. The high correlation coefficient R^2 obtained from pseudo-second model indicates it suitability when compared to the pseudo-first order model. In addition the $q_{e,cal}$ obtained from the pseudo-second order model was close to the experimental value, $q_{e,\,exp}$. This is an indication of suitability of the pseudo-second order model in characterising the adsorption of EBT on the materials.

4.5 Effect of Temperature and Thermodynamic studies

Thermodynamic study was undertaken to know the effects of temperature on the adsorption process via changes in enthalpy (ΔH), Gibb's free energy (ΔG) and entropy (ΔS) according to the following relation

$$\Delta G = -RT\ lnK_D \qquad 4.1$$

$$lnK_D = \frac{\Delta S}{R} - \frac{\Delta H}{RT} \qquad 4.2$$

where K_D defines distribution coefficient, T is absolute temperature and R is molar gas constant. The thermodynamic variables are documented in Table 4.3. The adsorption of EBT on all the as-synthesized samples is thermodynamically feasible and spontaneous with strong affinity between the adsorbate and the adsorbents as indicated by a negative value of ΔG [81]. In addition, the adsorption is exothermic as the adsorption performance

Table 4.2 Parameters of kinetic models

Adsorbent		Pseudo first order			Pseudo second order		
	$q_{e\ (exp)}$	$q_{e(cal)}$	k_1	R^2	$q_{e(cal)}$	$k_2 * 10^{-2}$	R^2
NMA	118.50	72.23	0.0060	0.95	111.11	2.95	0.99
G/NMA	124.76	37.162	0.0067	0.95	120.48	8.87	0.99
NMA-C	134.34	106.29	0.0081	0.93	161.29	0.76	0.96
G/NMA-C	137.02	39.26	0.0108	0.90	138.88	7.86	0.99

Table 4.3 Thermodynamics Parameters for adsorption of EBT

Sample	T(k)	K_d	ΔG	ΔH	ΔS
NMA	298	14.38	6.60	-10.63	-14.08
	308	10.42	6.00		
	323	10.13	6.23		
NMA-C	298	11.07	5.96	-20.01	-46.62
	308	10.11	5.92		
	323	6.03	4.82		
G/NMA	298	5.87	4.39	-6.58	-7.70
	308	4.83	4.03		
	323	4.73	4.17		
G/NMA-C	298	20.40	7.47	-30.96	-80.58
	308	8.25	5.40		
	323	7.35	5.36		

declines with increase in temperature as noticed with a negative ΔH. The negative ΔS indicated higher order of reaction took effect on adsorption of EBT on the samples.

4.6 Adsorption Mechanism

Fig 4.9 shows the XRD of the used adsorbents which shows a slight shift in the positions of diffraction peaks when compared to fresh samples (Fig 1). This suggest partial intercalation of EBT into the structure with a removal via surface adsorption. The XRD patterns of used calcined samples display peaks assigned to d_{003} and d_{006} similar original LDHs XRD patterns which forms through rehydration and surface reconstruction upon contact with aqueous solution. The peaks were broad with decreased intensity implying reduced crystallinity. The calcined samples regained their original LDHs structure through memory effect upon rehydration. Structural reconstruction via 'memory effect' with partial intercalation of anionic species along with surface adsorption forms the basis of dye removal by calcined LDH and hybrid.

Fig 4.10 shows the FTIR of the spent adsorbent which display that the bands were weak especially the strong nitrate band. This suggest anion exchange of NO_3^- by dye molecules. Other additional peaks observed were from EBT and this shows that the dye was adsorbed onto the surfaces of the adsorbents. Fig 4.11 shows microstructure of samples after EBT adsorption. It is vivid that the irregularly shaped rough surfaces transform to smooth surfaces with slight irregularities. A closer look at the SEM images of Fig 4.13 shows the incorporation of EBT onto the LDH, hybrid LDH and its calcined nanocomposites. It is proposed that mechanism behind the adsorption process are ion exchange and surface adsorption for uncalcined samples while structural reconstruction, ion exchange and surface adsorption were involved for the calcined samples.

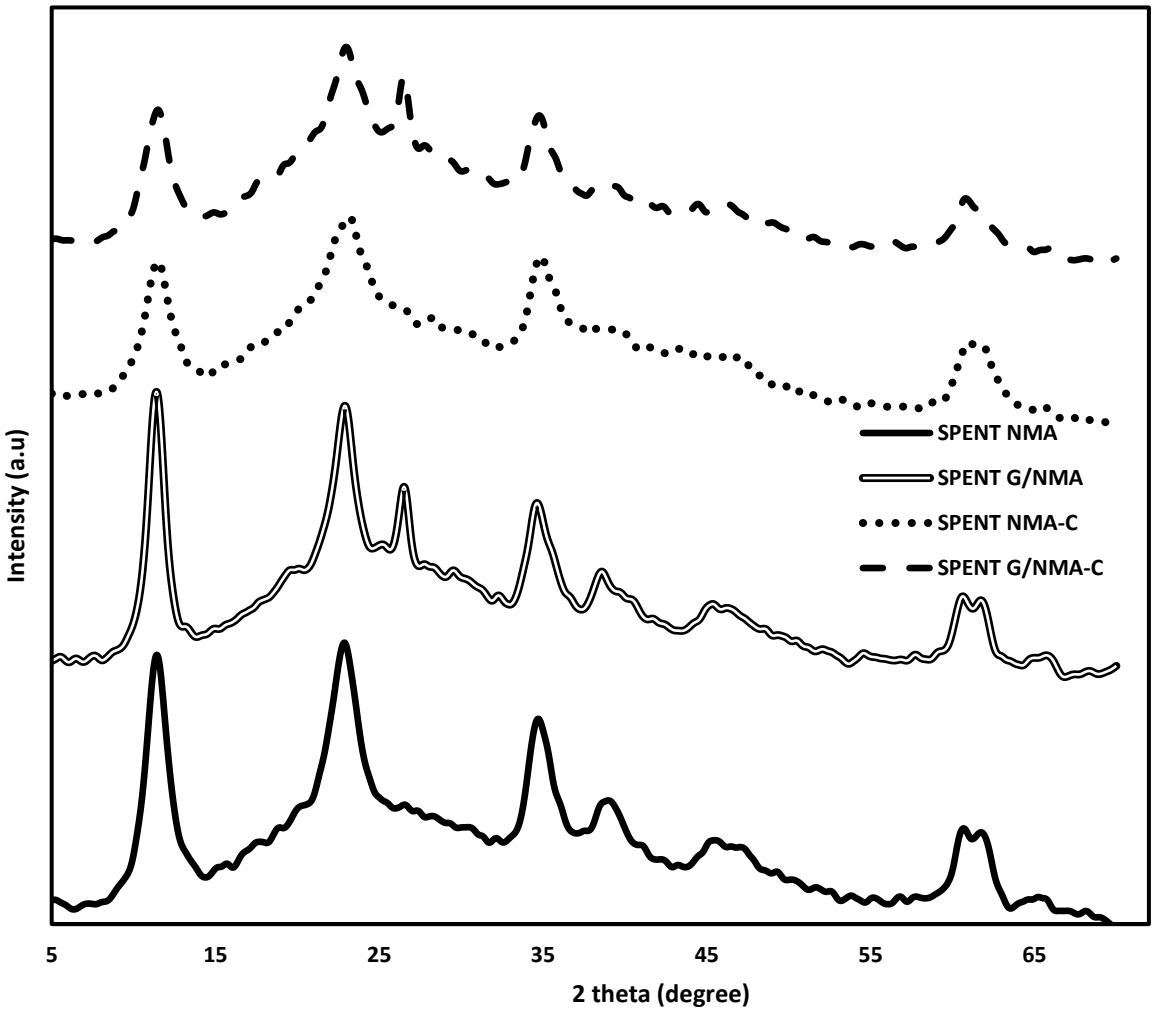

Fig 4.9 XRD of spent NMA, G/NMA, NMA-C and G/NMA-C.

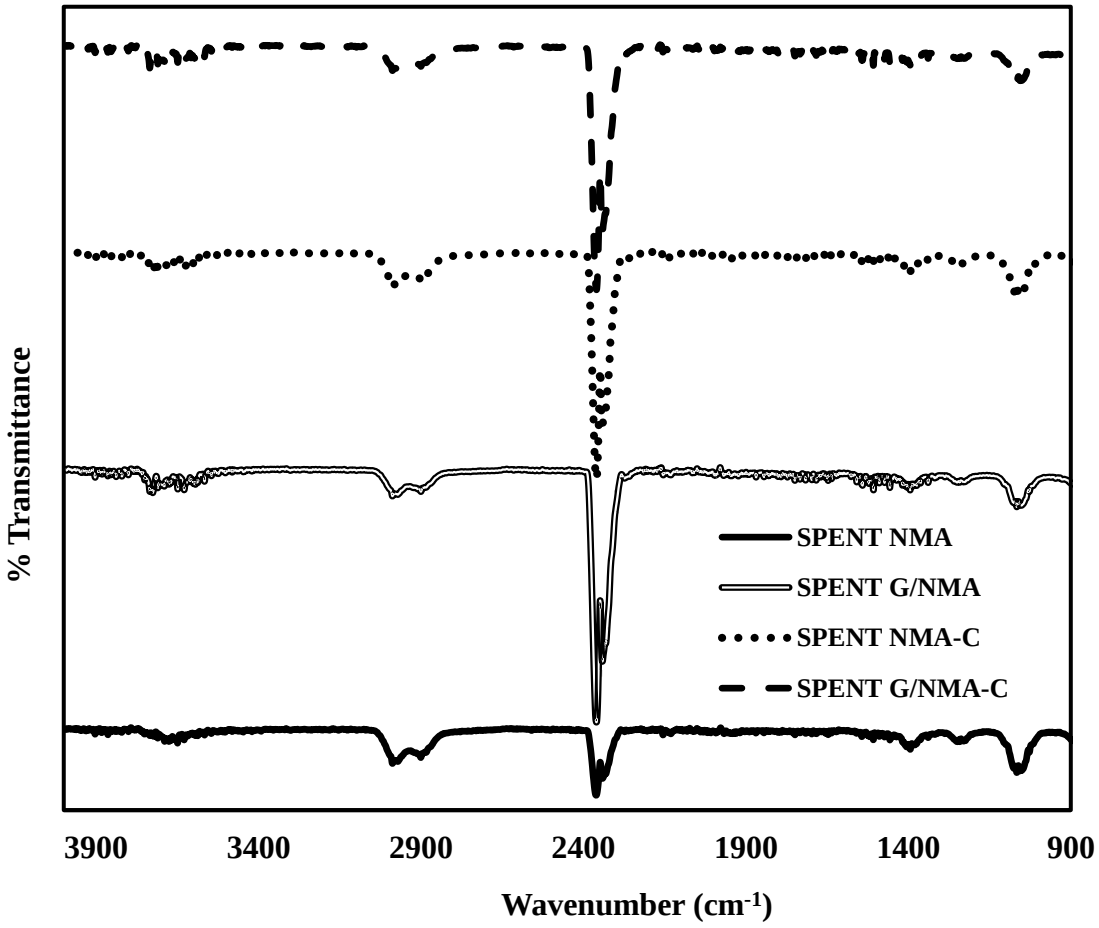

Fig 4.10 FTIR of spent NMA, G/NMA, NMA-C and G/NMA-C.

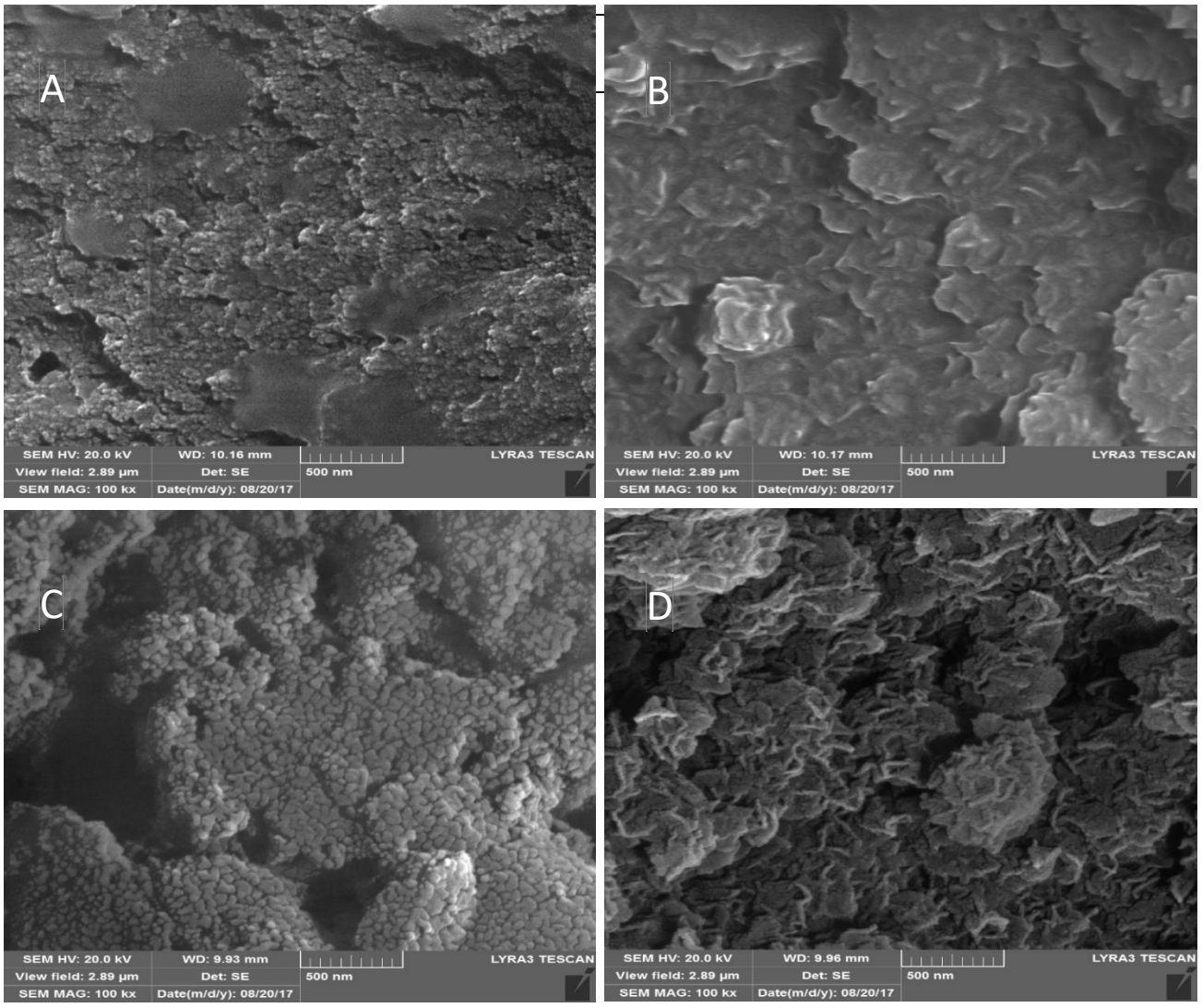

Fig 4.11 SEM of spent (A) NMA (B) G/NMA (C) NMA-C and (D) G/NMA-C.

4.7 Regeneration and Reuse of Adsorbents

Regeneration and reuse account for substantial part (> 70%) of operating and maintenance cost [82, 83], hence great consideration is given towards choosing materials for economic feasibility of any process. Due anionic nature of the dye, alkaline solution can desorb the dyes molecules by weakening the electrostatic attraction between the surfaces of adsorbents and the dye [84]. 0.1M NaOH solution was employed to regenerate the LDHs and graphene hybrid. In addition to the basic treatment, calcination at 500^0C for 4h under nitrogen environment was used to regenerate the calcined NiMgAl and its graphene hybrid. For subsequent regeneration, the same desorption and calcination treatments were employed. Fig 4.12 shows EBT dye removal after each cycle reuse and regeneration. On NMA, the percentage of EBT removed decreased from 88% to 81% in the first 2 cycles and reached 57% at the end of the fourth cycle. G/NMA reached 74% removal efficiency at the end of the fourth cycle. This less reduction may be due to the influence of graphene in the LDH structure. After regeneration, lower peaks were observed implying decreased crystallinity of LDHs which explains the reduction in adsorption performance. Calcination helped improved the recovery of the adsorbent as calcined NiMgAl and Graphene-NiMgAl had percentage removal of 80% and 87% at the end of the forth cycle. This implies the regeneration of the adsorbents were efficient and they could be deployed as affordable reusable adsorbents.

4.8 Comparison with Other adsorbents

Table 4.4 compares the maximum adsorption capacity of the adsorbents synthesized in the work with other conventional adsorbents previously reported in literature. It clearly shows that those from this work exhibit superior performances that others, implying it could be

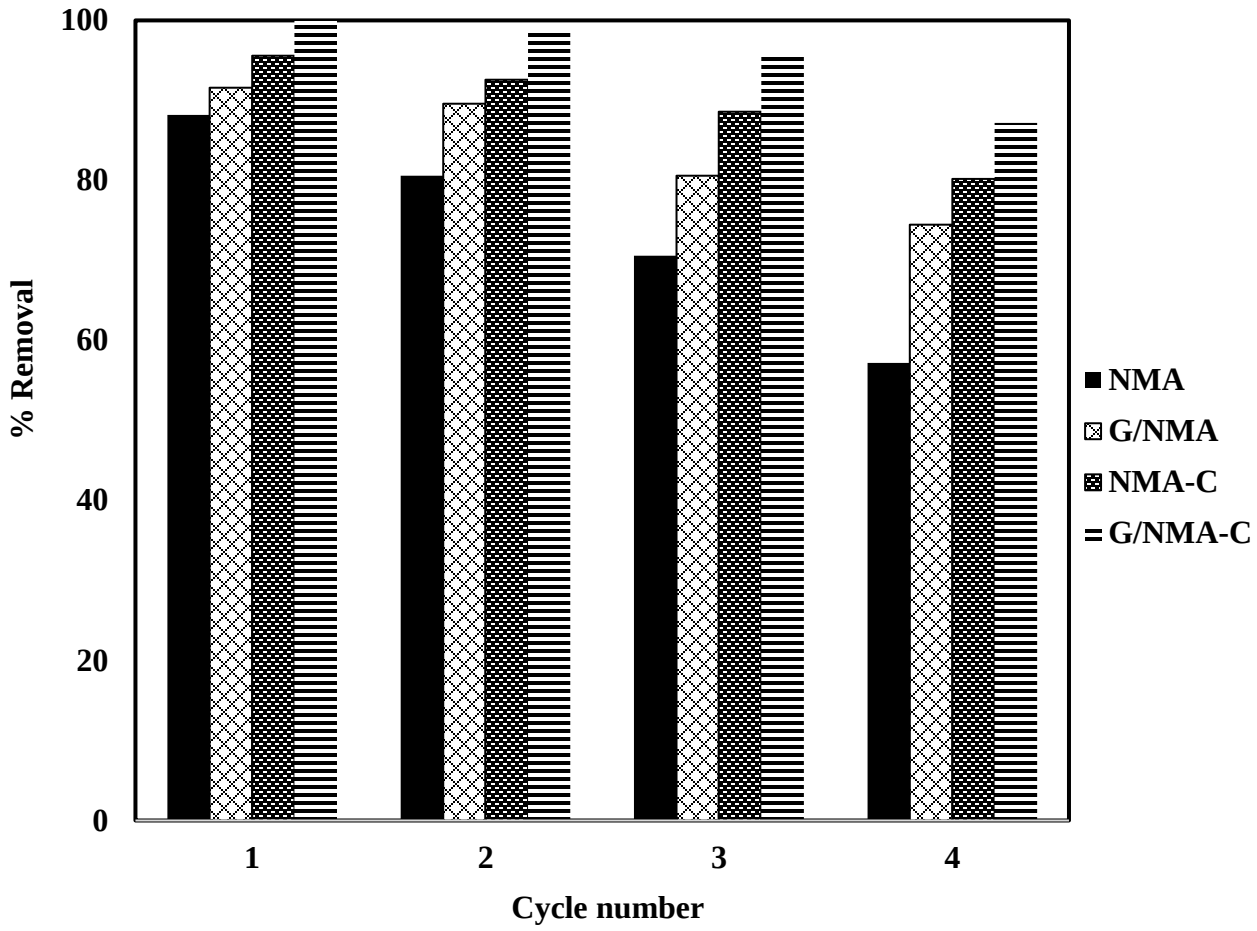

Fig 4.12 Percentage removal of EBT Dye adsorbents after four regeneration cycles.

Table 4.4 Comparison of Adsorption capacity and Parameters of various Adsorbents

Adsorbent	pH	Time, Temp	models	Q_m (mg/g)	references
Bottom ash	3.5	270/40	Langmuir/ 2nd	94.122	[85]
Activated carbon	2		Freundlich/2nd	160	[86]
Almond shell MW irradiated	4	180/30	Lang/ 2nd	29.41	[87]
MgAl- LDH	2-4		Lang/2nd	128	[49]
Eucalptus Bark	2	-/30		52.36	[88]
Maize stem	2		Lang/ 2nd	167.84	[89]
NMA	4	240	Langmuir/ 2nd	156.25	This work
G/NMA	4	90	Langmuir/ 2nd	263.16	This work
NMA-C	4	180	Langmuir/ 2nd	238.14	This work
G/NMA-C	4	60	Langmuir/ 2nd	384.62	This work

deployed for the remediation of anionic dye contaminated water. The higher performances may be attributed to the synthesis techniques which facilitated the formation of abundant function groups of oxygen and higher surface area resulting from calcination [90, 91] was further improved by hybridizing the LDHs with graphene.

CHAPTER 5

Graphene/ Ternary Layered Double Hydroxide Nanocomposites For Efficient Removal Of Methyl Orange From The Aqueous Phase

The chapter reports the result of adsorption of Methyl orange (MO) on the ternary LDH and its nanocomposite from the aqueous phase. For simplicity, uncalcined MgCoAl, calcined MgCoAl, uncalcined graphene-MgCoAl and calcined Graphene-MgCoAl are referred to as MCA, MCA-C, G/MCA and G/MCA-C respectively.

5.1 Characterization of MCA, G/MCA, MCA-C and G/MCA-C

LDHs possess unique characteristic diffraction peaks [69, 92] which are well established in the ternary LDH as presented in Fig 5.1. The intensity of the symmetric peak at 11.36^0 assigned to the (003) plane indicates a well-defined crystalline structure with associated basal spacing of 0.775nm. The other peaks at $2\Theta = 22.9^\circ$, 34.5°, 38.9°, 45.5°, 60.3°, and 61.5° are indexed to the (006), (009, (015), (018, (110) and (113) respective planes. The pristine graphene shows its peak at 26.84° 2Θ assigned to the 002 plane [70, 93]. The G/MCA maintains a similar structure to MCA due to the occurrence of similar 110 and 113 peak planes [94] but with graphene induced broadness in the (003) and (006) planes of G/MCA. The broadness may be ascribed to the occurrence of electrostatic interaction in the composite which affected the nucleation and crystallize size of the LDH [95]. Similar observations have been previously reported [94]. Upon calcination, the LDHs peaks

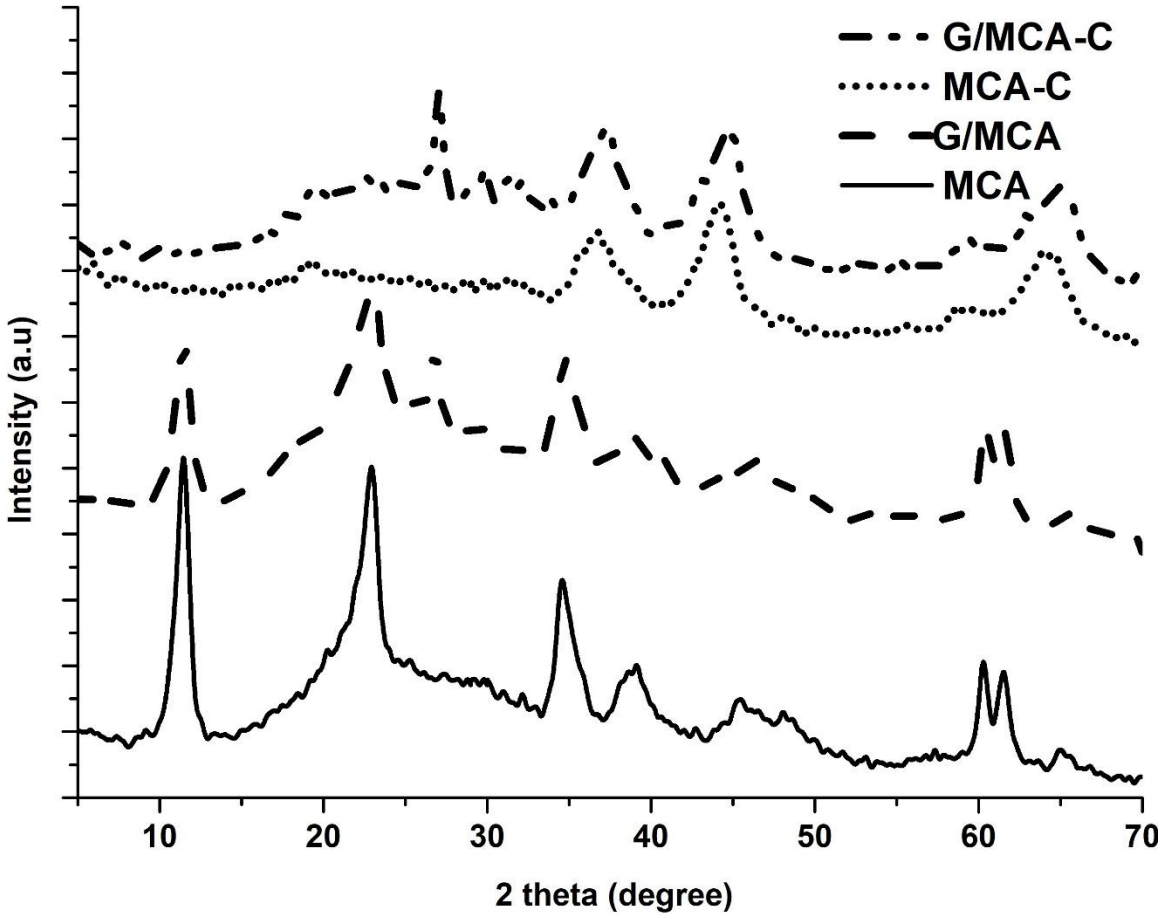

Fig 5.1 XRD of MCA, G/MCA, MCA-C, and G/MCA-C

become alienated due to destruction of its structure resulting in formation of mixed metal oxides (MMO) known with peaks located at the (111), (200) and 220 planes [10, 52].

FTIR analysis is an important tool to help understand the active sites and interactions of group responsible for the adsorption. Fig 5.2 depicts the FTIR of MCA, G/MCA, MCA-C and G/MCA-C. For MCA and G/MCA, the peaks between 3400 and 3600 cm^{-1} are assigned to the stretching modes of the interlayer water molecule while the bending modes of water are located at 1640 cm^{-1} [96]. In addition, the interlayer anions (NO_3^-) have a stretching peak at 1350 cm^{-1} while the peaks below 1000 cm^{-1} corresponds to the metal-oxygen vibration bond [92]. Vibration relating to the C-O-C bond is located at 1040 cm^{-1}. Calcination led to removal of interlayer and physisorbed water molecules and interlayer anions and this is evident in peak reduction in both MCA-C and G/MCA-C. This further confirm the alteration of the structure of the LDHs as previously established by XRD. Calcination helps with more production of oxygen containing functional groups which is expected to profoundly increase the MO adsorption capacity [97].

Thermal behaviors and temperature dependent decomposition patterns of the synthesized samples were investigated by thermogravimetry analysis (TGA) under nitrogen environment up to 800°C as shown in Fig 5.3. MCA and G/MCA experience three modes of weight losses which resulted in total weight reduction by 39% and 37.7% respectively. Physisorbed and intercalated water molecules are removed up to a temperature below 200°C in the first stage [98] and this accounts for 10.4 and 8.5% loss. This is subsequently followed by dihydroxylation (DH), decarbonation (DC) and removal of other interlayer anions such as nitrates in the second stage of weight loss between 200°C and 400°C and this resulted in 23.3 % loss for both. The third stage involves little weight beyond 400°C

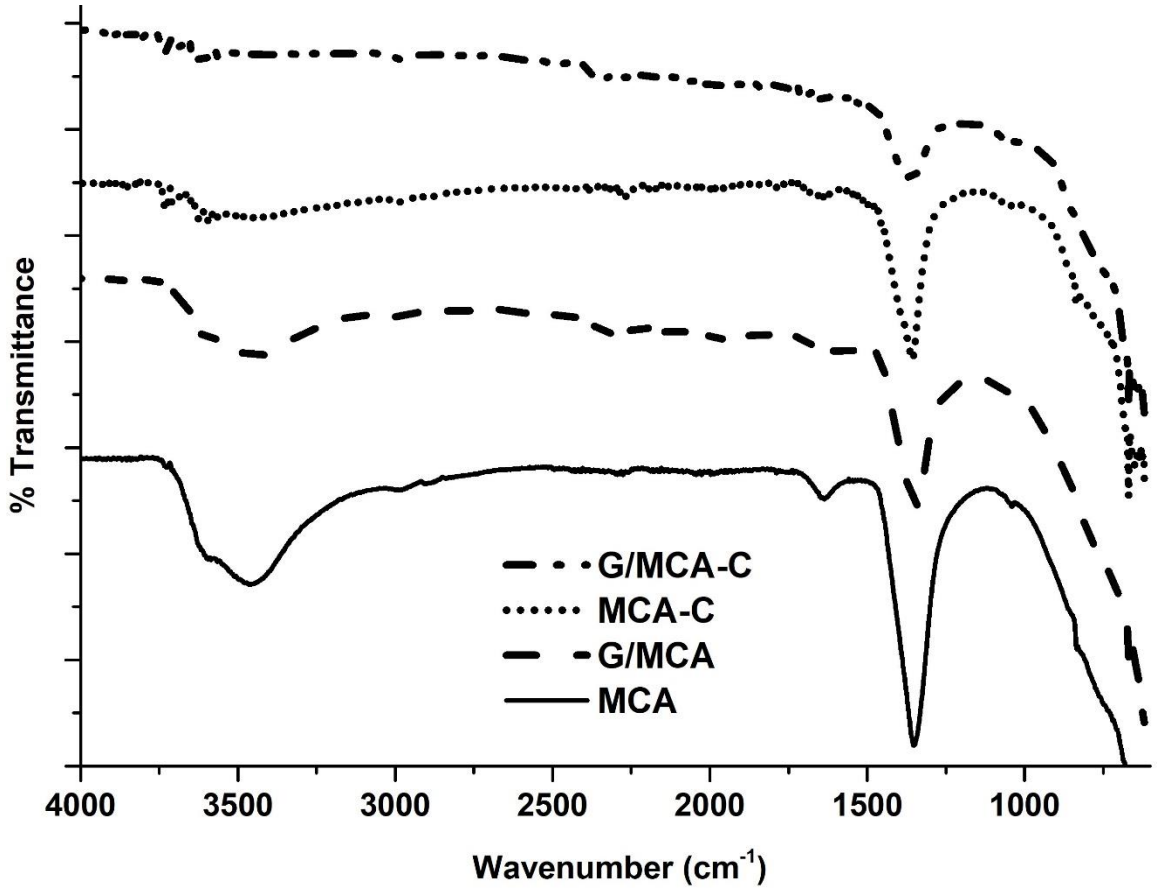

Fig 5.2 FTIR of MCA, G/MCA, MCA-C, and G/MCA-C

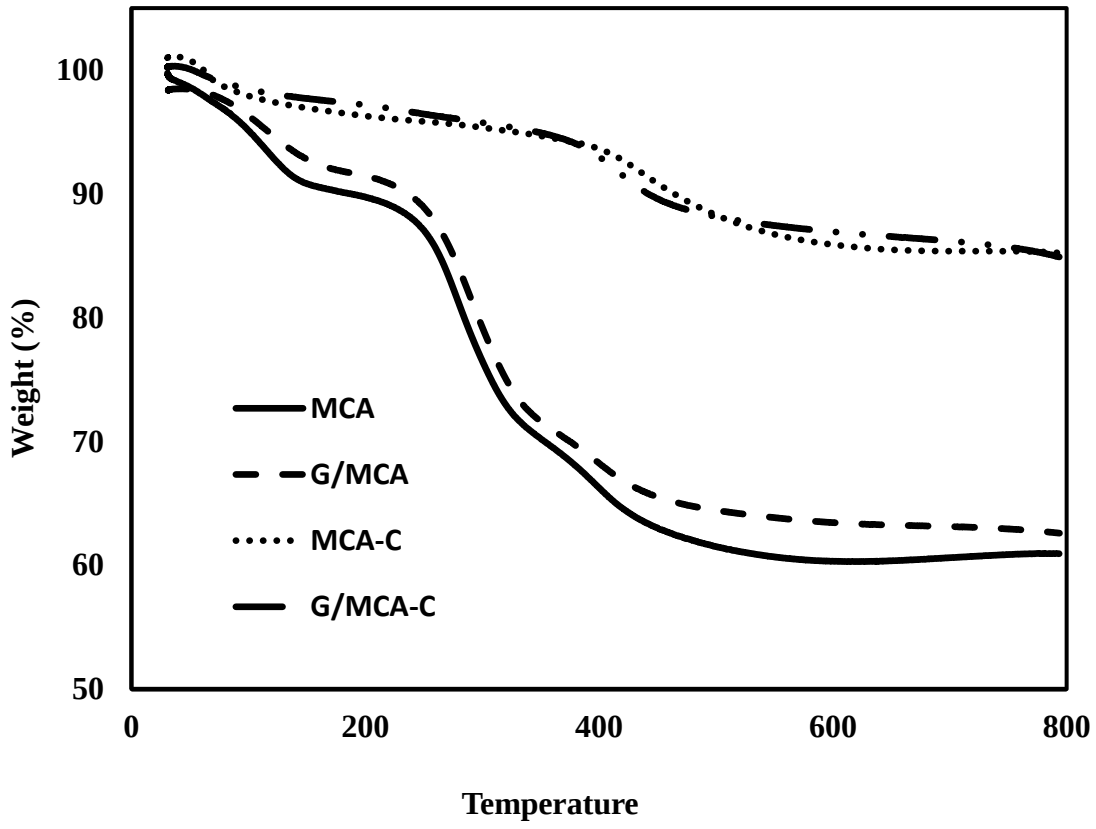

Fig 5.3 TGA of MCA, G/MCA, MCA-C and G/MCA-C

with further decarbonation and dehydroxylation results in production of mixed metal oxides (MMO) [99]. MCA-C and G/MCA-C experience two modes of weight reduction which are mainly due to DC and the interlayer anions removal and formation of MMO. Most of the water molecules have being eliminated due to calcination. Between (35°C and 40°C), both MCA-C and G/MCA-C gained weight due to absorption of water molecules from the environment and these were subsequently removed with increase in temperature

The SEM microstructures images of the adsorbent samples are shown in Fig 5.4. The SEM of MCA shows large numbers of loose flower-like nanoparticles which are uniformly distributed. The morphology observed is a result of the synthesis route which has previously been reported [100]. Introduction of graphene to form G/MCA resulted in the formation of irregularly shaped plate-like nanosheets with overlapping configuration. The calcination resulted in the formation of the adsorbents with rough and compact surfaces.

5.2 Adsorption Parameters

Effects of parameters such as pH, contact time, adsorbent dosage, EBT concentration and temperature were studied

5.2.1 Effect of Initial pH

The surface charge, active sites dissociation of functional group of the adsorbent, extent of ionization and structure of the dye molecules are predominantly affected by pH [41, 45]. The percentage dye removal dependence on ph when the pH was varied from 3 to 9 is shown in Fig 5.5 (A) meanwhile Fig 5.5 (B) displays the point of zero charge (ph_{PZC}) of MCA, G/MCA, MCA-C and G/MCA-C determined by the drift method [73]. The ph_{PZC} of MCA, G/MCA, MCA-C and G/MCA-C are 4.99, 5.17, 5.94 and 5.94 respectively. The

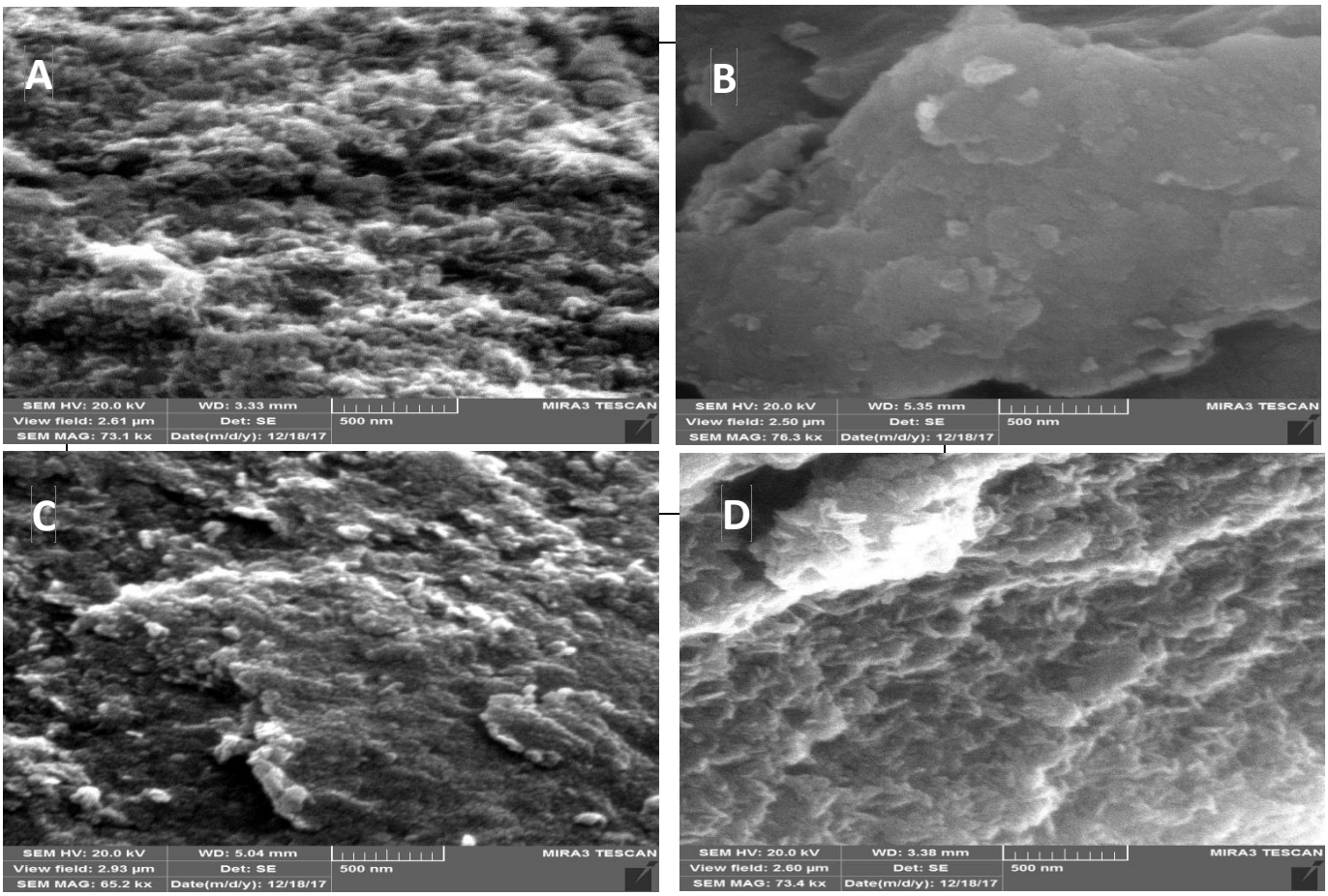

Fig 5.4 SEM of (A) MCA, (B) G/MCA, (C) MCA-C, and (D) G/MCA-C

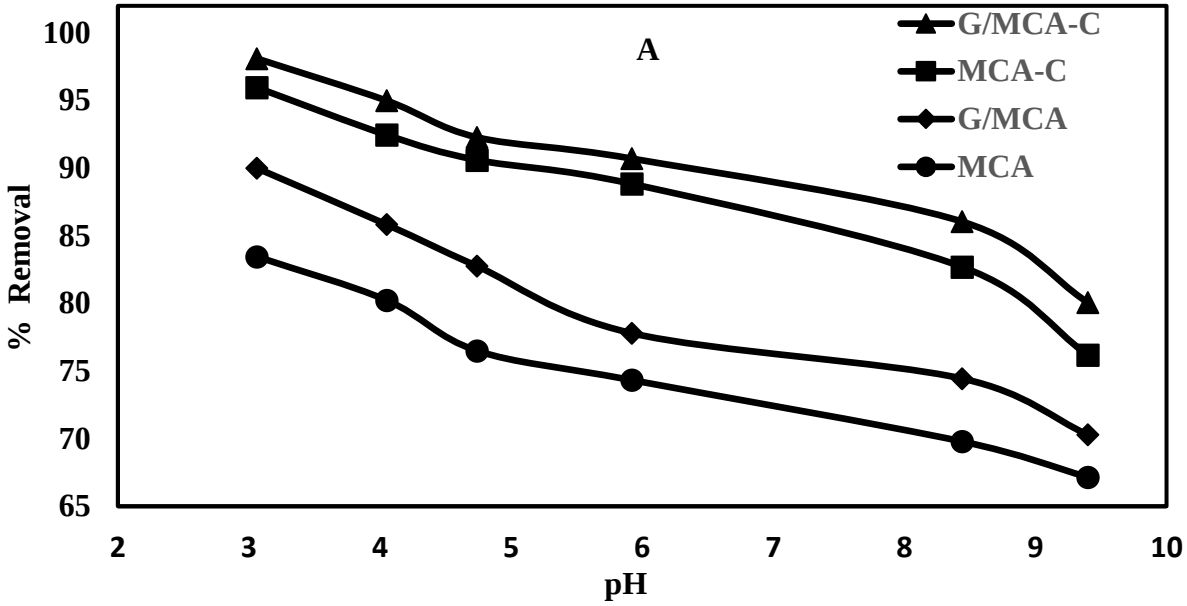

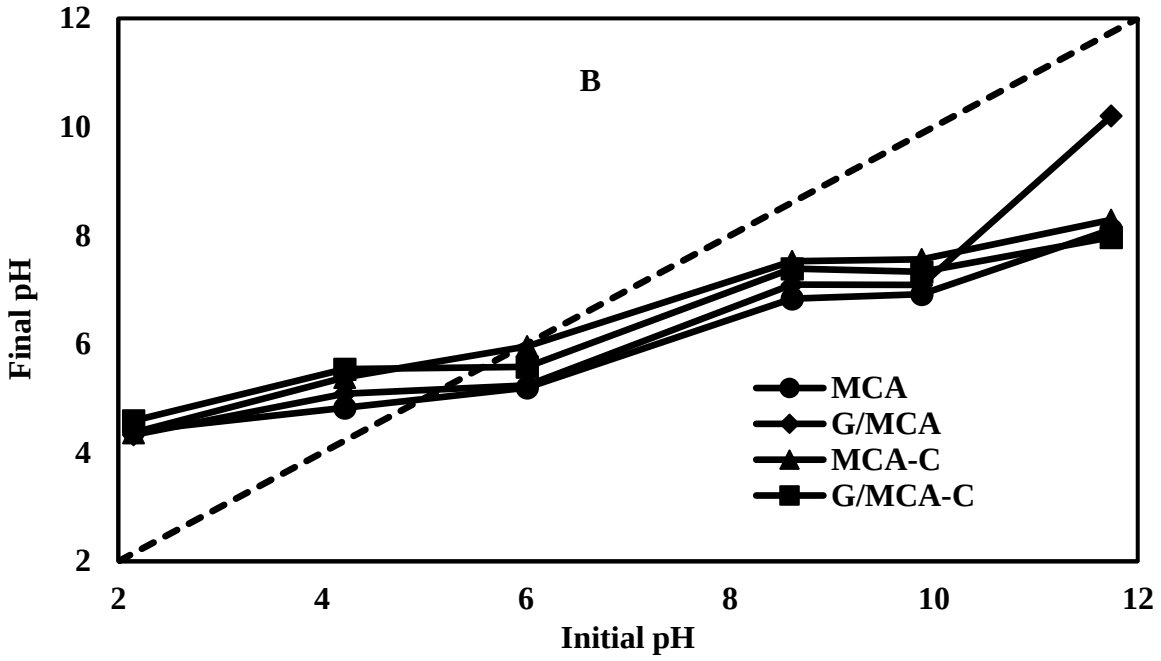

Fig 5.5 (A) Effect of pH on percentage removal of MO at 298K. C_0 = 30 mg/L; dosage = 10 mg (B) pH_{PZC} for MCA, G/MCA, MCA-C and G/MCA-C

MO percentage removal was observed to decline for a rise in pH from 3 to 9 and this trend is experienced by all the adsorbents. Similar behavior were associated with other LDH as reported elsewhere [98].

Surface charges of the adsorbents in the aqueous medium can be used to substantiate this behavior. For pH 3 below the pH_{PZC}, the adsorbents possess positively a charged surface (protonated) which enhances electrostatic attraction to negatively charged molecules of the anionic dyes. Hence, the highest removal of the dye of 83, 88, 96 and 98% for MCA, G/MCA, MCA-C and G/MCA-C respectively, was achieved at pH 3. As the pH increased to pH 4 and above, there was a reduction in the number of positively-charged adsorption sites leading to decreased removal of MO molecules. Furthermore, increasing the pH beyond ph_{PZC} led to formation of a negatively charged adsorption surface which stimulates electrostatic repulsion between the anionic dye molecules and adsorbents. However, at a higher pH (>> pH_{PZC}), increased competition between dyes molecules and OH^- in aqueous solution in addition to electrostatic repulsion profoundly reduced the percentage dye removal [15]. Consequently, pH 3 was used for the subsequent adsorption studies presented below.

5.2.2 Effect of Dosage

The variability of percentage MO removal when MCA, MCA-C, G/MCA and G/MCA-C adsorbents dosages were varied from 2 mg to 25 mg is shown in Fig 5.6. The percentage removal increases with increase in adsorbent dosage for all the adsorbents. The percentage removal increased from 28, 31, 51, and 57% to 72, 78, 92, and 96% for a change in dosage from 2 mg to 8mg for MCA, MCA-C, G/MCA and G/MCA-C respectively. These increments can be ascribed to increased supply of active adsorption sites. The highest

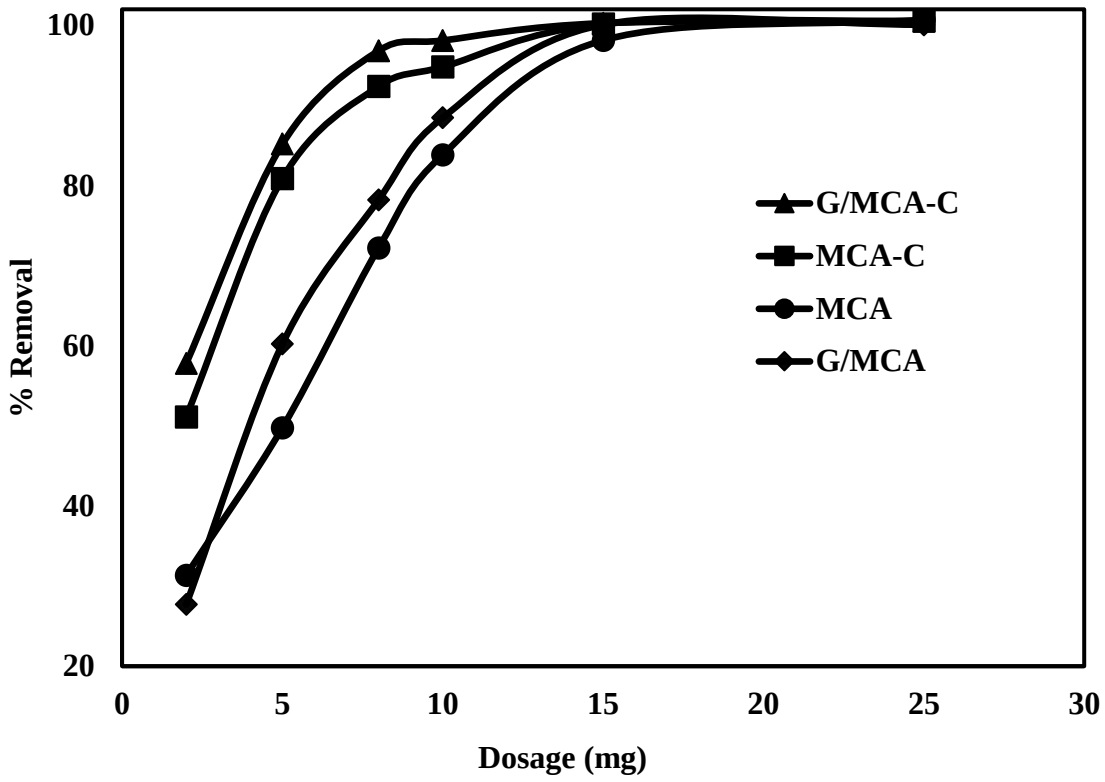

Fig 5.6 Effect of dosage on percentage removal of MO at 298K. Contact time= 180mins; C_0 = 30 mg/L

adsorption was experienced by G/MCA-C. This was attributed to the interplay of graphene introduction and calcination considering that the least removal was associated with the MCA. Beyond 10mg, there was a differential change in percentage removal of the MO with dosage which indicates the satiation of the quantity of MO molecules by the increased active adsorption sites. Thus, 10 mg was selected as the optimum dosage and was used for subsequent experimentation.

5.2.3 Effect of Contact time

The influence of contact time varied from 15 minutes to 1440 minutes on percentage removal of MO for all the MCA, G/MCA, MCA-C and G/MCA-C is shown in Fig 5.7. All four adsorbents exhibited fast sorption in the first 15 minutes with measured removal efficiency of 60, 67, 57 and 85 % for MCA, G/MCA, MCA-C and G/MCA-C respectively. The MO removal increased with higher contact time until equilibrium was established at 240, 240, 180 and 180 minutes for MCA, G/MCA, MCA-C and G/MCA-C respectively. The fast adsorption of calcined samples in the first few minutes can also be attributed to memory effect [79]. The higher adsorption of G/MCA over MCA can be ascribed to the contribution of graphene which improved the properties of the nanostructured G/MCA. However, the higher adsorption of MCA-C over MCA was attributed to calcination which enhances the availability of oxygen carrying functional groups. Thus, both the interplay of graphene introduction and calcination leads to the highest adsorption experienced by the G/MCA-C. In addition, the abundance of oxygen-carrying functional group also contributes to fast adsorption of the dye [98].

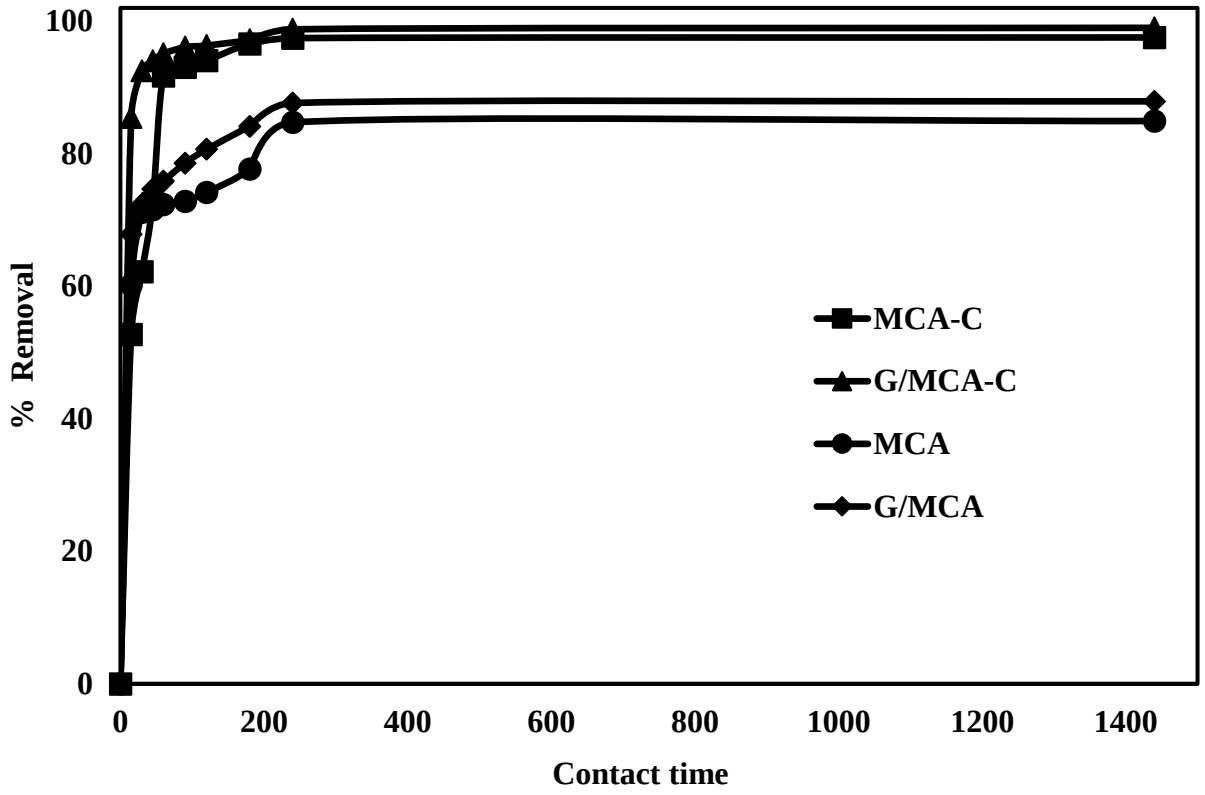

Fig 5.7 Effect of contact time on percentage removal of Methyl orange. Adsorbent dosage 10mg; C_0 = 30 mg/L

5.2.4 Effect of initial MO concentration

Influence of initial dye concentration on percentage removal of MO is depicted in Fig 5.8. The plot shows that there was reduction in percentage removal as initial concentration was increased. When the MO concentration was increased at a fixed adsorbent dosage, active sites were also fixed in number are occupied and free active binding sites are continuously been filled up. Hence, unadsorbed dye molecules are left in the solution after complete occupation of adsorption sites. At 30 mg/L MO concentration, the percentage removal of MO of 83, 88, 96 and 98 were significantly, decreased to 60, 65, 75% and 77% when the concentration was increased to 150 mg/L for MCA, G/MCA, MCA-C and G/MCA-C, respectively, for a fixed dosage of 10 mg for a contact time of 180 min. Further increases in the MO concentration induced more reduction in the MO percentage removal. As previously observed, G/MCA-C experienced the highest adsorption of all initial MO concentrations due to the synergistic interplay previously explained.

5.3 Adsorption Isotherm

An adsorption isotherm study is significant in designing adsorption system due to its importance in estimating the adsorbent adsorption capacity as well as analyzing interaction between adsorbate and adsorbent at equilibrium [77]. Thus, two common adsorption isotherm models, Langmuir and Freundlich, are used to model the four investigated adsorbents adsorption processes. The Langmuir isotherm is considered accurate on the premise that the adsorption occurred on monolayer surfaces with equivalent energies, no interaction occured among adsorbed molecules and the same adsorption mechanism is experienced by all molecules [36]. The Langmuir model is given as

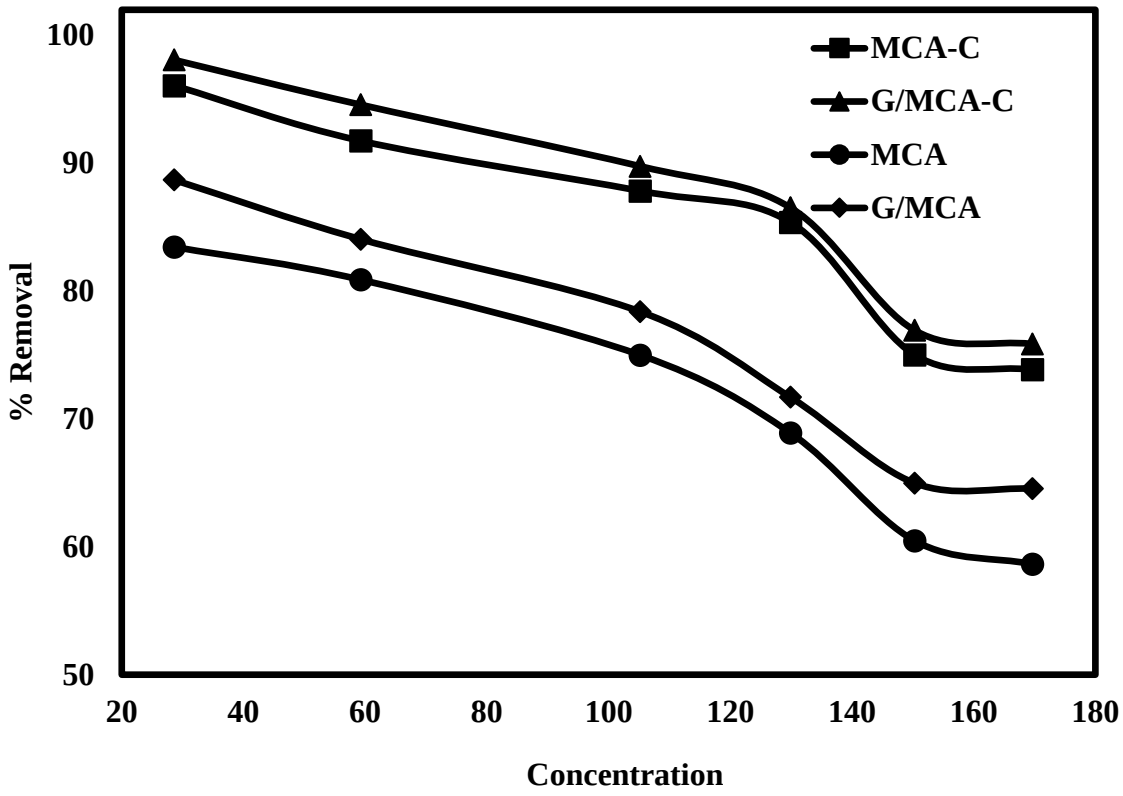

Fig 5.8 Effect of concentration on percentage removal of MO at 298K. Contact time= 180mins; adsorbent dosage= 10 mg

$$q_e = \frac{q_m\, b\, C_e}{1 + b\, C_e} \qquad 5.1$$

Where q_m (mg/g) and b (L/mg) are Langmuir constants signifying maximum monolayer adsorption capacity and a parameter relating to free energy of adsorption respectively[41]. Linearizing equation 5.1 gives

$$\frac{C_e}{q_e} = \frac{1}{b\, q_m} + \frac{C_e}{q_m} \qquad 5.2$$

The value of b and q_m are obtained from the intercept and slope respectively of the linear plot of C_e versus q_m in equation 5.2. Another parameter termed the separation factor, R_L, defined in Chen et al. [60] signifies unfavourable, linear, favourable, and irreversible adsorption at $R_L > 1$, $R_L = 1$, $0 < R_L < 1$ and $R_L = 0$ respectively.

$$R_L = \frac{1}{1 + b\, C_0} \qquad 5.3$$

On the other hand, the Freundlich isotherm assumes a multi-layered heterogeneous adsorption with heat of adsorption distribution [43] and its non-linear and linear forms are given in equation 7 and equation 8, respectively.

$$q_e = K_F\, C_e^{1/n} \qquad 5.4$$

$$\log q_e = \log K_F + \frac{1}{n} \log C_e \qquad 5.5$$

Where n and K_f are Freundlich constants indicating adsorption intensity and distribution coefficient relating to bonding energy respectively [69]. 1/n < 1 indicates a normal Langmuir isotherm while 1/n > 1 is cooperative adsorption [80]. The value of 1/n and K_F

are obtained from the slope and intercept, respectively, of the linear plot of $\log q_e$ versus $\log C_e$ in equation 5.5.

Table 5.1 shows the parameters of adsorption of both Langmuir and Freundlich isotherms models. It is apparent that the correlation coefficient of the Langmuir model ($R^2 > 0.98$) is higher than that of the Freundlich model indicating that the former more closely fits the adsorption process when compared to the latter. This assertion was adequately, corroborated considering the values of 1/n (1/n < 1). Likewise, the values of R_L ($0 < R_L < 1$) indicate the favorability of the adsorption process for all the four adsorbents. The drop in maximum adsorption capacity with increases in temperature indicates the unfavorability of the adsorption at higher temperatures. Moreover, the maximum adsorption capacity at 25°C is 357.14, 384.62, 400 and 434.78 mg/g for MCA, G/MCA, MCA-C and G/MCA-C, respectively. It can be concluded that the adsorption is majorly characterize by homogeneity as depicted by the close fit of the Langmuir model.

5.4 Adsorption Kinetics

Kinetic models are essential in predicting sorption rate and expressing a suitable reaction mechanism [101]. Thus, the linearized forms of both pseudo-first order (equation 5.6) and pseudo-second order (equation 5.7) models are fitted to the experimental data. The best model describing the MO adsorption kinetics for the adsorbents was determined by considering the model with highest coefficient of correlation (R^2)

$$log(q_e - q_t) = \ logq_e - \frac{k_1\, t}{2.303} \qquad 5.6$$

$$\frac{t}{q_t} = \ \frac{1}{k_2\, q_e^2} + \frac{t}{q_e} \qquad 5.7$$

Table 5.1 Parameters of Isotherm models for adsorption of Methyl orange

Sample	T (K)	Langmuir			Freundlich		
		Q_m (mg/g)	R_L	R^2	K_F	1/n	R^2
MCA	298	357.14	0.0932	0.9930	35.7026	0.5190	0.9423
	308	312.50	0.0873	0.9838	34.1350	0.4958	0.9041
	318	208.33	0.0455	0.9720	38.6634	0.3841	0.7828
G/MCA	298	384.62	0.0782	0.9958	45.2585	0.4908	0.9714
	308	344.83	0.0806	0.9936	40.1051	0.4872	0.9374
	318	256.41	0.0580	0.9767	39.6552	0.4282	0.8213
MCA-C	298	400.00	0.0331	0.9944	81.6770	0.4190	0.9627
	308	384.62	0.0291	0.9829	62.1727	0.4805	0.9444
	318	357.14	0.0655	0.9928	46.7951	0.4768	0.9198
G/MCA-C	298	434.78	0.0420	0.9783	106.6596	0.3570	0.9771
	308	400.00	0.0337	0.9973	77.9292	0.4328	0.9246
	318	370.37	0.0580	0.9961	52.7715	0.4655	0.9347

Where k_1 (min^{-1}) and k_2 (g mg^{-1} min^{-1}) are constants from pseudo-first order and pseudo-second order models respectively. Both constants are obtained from the linear regression of their respective equations. The parameters of both models are contained in Table 5.2. From the tabulated result, it is deduced that the pseudo-second order model (R^2> 0.99) adequately fits the experimental data. Also, the maximum adsorption capacity from the pseudo-second order model closely matches the experimental value. It can be stated that rate controlling mechanism of the adsorption is predominated by chemisorption which is the basic assumption the pseudo-second order model was built on [102]. Similar results have been published indicating chemisorption as the controlling step in removal of many dyes by LDHs [33, 98, 100, 101].

5.5 Thermodynamics and Effect of Temperature

The effect of temperature and change in internal energy relating to adsorption processes are important and they can be provided from thermodynamic consideration through changes in enthalpy (ΔH), Gibb's free energy (ΔG) and entropy (ΔS) according to the following relationship,

$$\Delta G = -RT\ lnK_D \qquad 5.8$$

$$lnK_D = \frac{\Delta S}{R} - \frac{\Delta H}{RT} \qquad 5.9$$

Where R (8.314 J/mol/K) is the molar gas constant and T (K) is the absolute temperature(K) .K_D (L/g) is a thermodynamic equilibrium constant obtained by plotting $\ln(q_e/C_e)$ versus qe and extrapolating q_e to zero [103]. ΔG is estimated from equation 11 while ΔH and ΔS are computed from the slope and intercept of the linear plot of $\ln K_D$ versus 1/T in equation 12.

Table 5.2 Parameters of Kinetic models

Adsorbent		Pseudo first order			Pseudo second order		
	$q_{e\ (exp)}$	$q_{e(cal)}$	k_1	R^2	$q_{e(cal)}$	$K_2 * 10^{-2}$	R^2
MCA	89.745	39.1832	0.01635	0.7221	90.0901	0.1101	0.9943
G/MCA	92.887	35.1480	0.01681	0.8621	94.3396	0.1186	0.9983
MCA-C	103.071	62.936	0.02556	0.9596	111.1111	0.0593	0.9972
G/MCA-C	104.607	12.779	0.0145	0.8921	105.263	0.3432	0.9999

In this study, three temperatures (298K, 308K and 318K) are considered to estimate the thermodynamic parameters. The values of the thermodynamic parameters are presented in Table 5.3 and the linear graph of ln K_D versus 1/T is shown in Fig 5.9.

Thus, these results indicate that the adsorption of MO by all the tested adsorbents is characterized by feasibility and spontaneity (negative ΔG) and are exothermic in nature (negative ΔH). This implies a decrease is adsorption and reduced spontaneity with increases in temperature as further suggested by the decreasing K_d being in agreement with increasing ΔG with increasing temperature [32, 103] . The negative values of ΔS for the four samples are an indication of reduced randomness at the absorbate/adsorbent interface and greater order of reaction associated with adherence of the dye on the surface of the adsorbents with a resultant reduction of the system's degree of freedom [104, 105].

5.6 Adsorption Mechanism

FTIR and XRD analyses of the spent MCA, G/MCA, MCA-C and G/MCA-C adsorbents were undertaken to understand the interaction of active sites on the adsorbent and functional groups of the dyes which can help better understand the adsorption mechanism [106, 107]. From the FITR results obtained as shown in Fig 5.10, it is obvious that new peaks appeared after the MO adsorption on all the adsorbents. A New band at 1118 cm^{-1} correspond to the C-N bond vibration while the band at 1031 cm^{-1} is ascribed to the symmetric stretching vibration of the $-SO_3^-$ of the MO [106, 108, 109]. This suggest that molecules of the MO dye are fastened on the surfaces of the adsorbents and that electrostatic interaction was involved in the process. It is also apparent that the peak of the NO_3^- vibration located at 1350 cm^{-1} on fresh adsorbents attenuated and slightly shifted to a higher wavenumber on the used adsorbents suggesting chemical interaction. The reduction

Table 5.3 Thermodynamic parameters for adsorption of Methyl orange

Sample	T(k)	K_d	ΔG	ΔH	ΔS
MCA	298	3.200	-2.882	-5.362	-8.281
	308	3.028	-2.837		
	318	2.792	-2.714		
G/MCA	298	3.615	-3.184	-7.181	-13.355
	308	3.360	-3.103		
	318	3.011	-2.914		
MCA-C	298	4.761	-3.866	-11.059	-24.124
	308	4.141	-3.639		
	318	3.595	-3.383		
G/MCA-C	298	5.649	-4.290	-15.179	-36.559
	308	4.600	-3.908		
	318	3.843	-3.559		

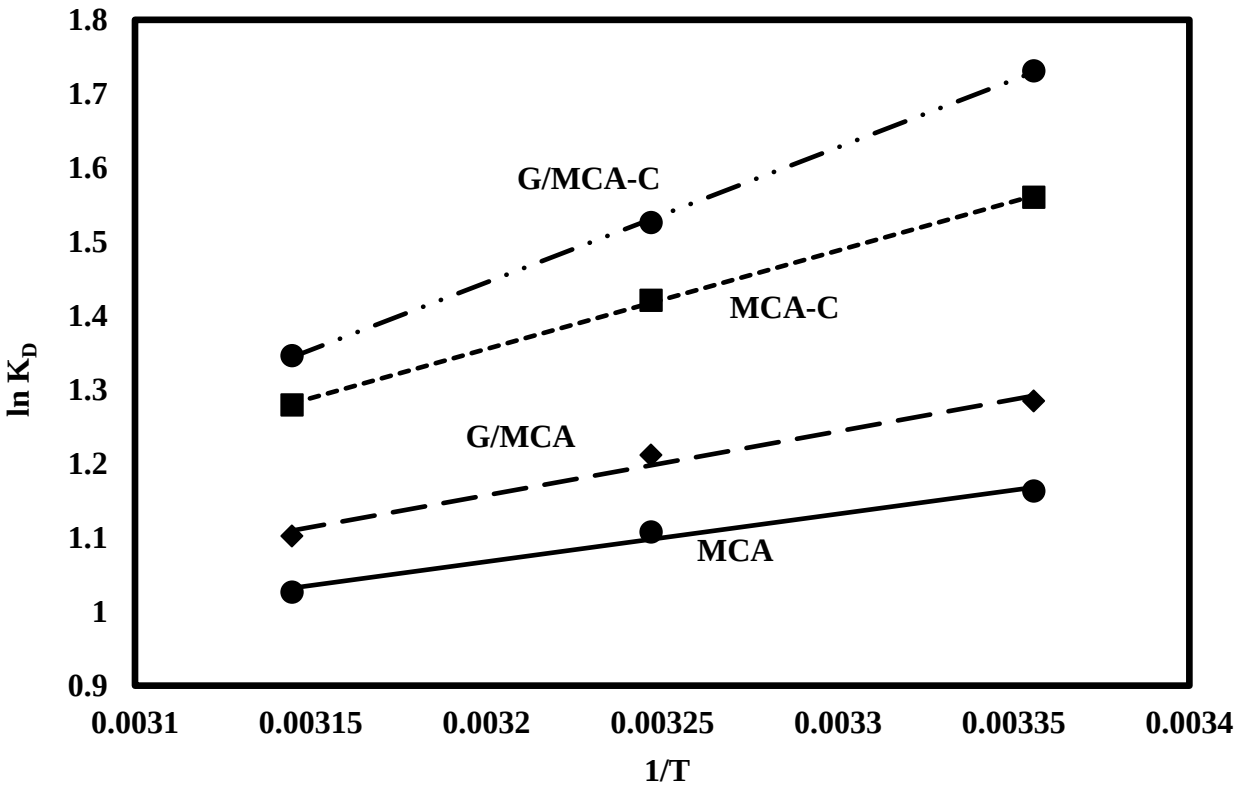

Fig 5.9 Linear plot of ln K_D vs 1/T

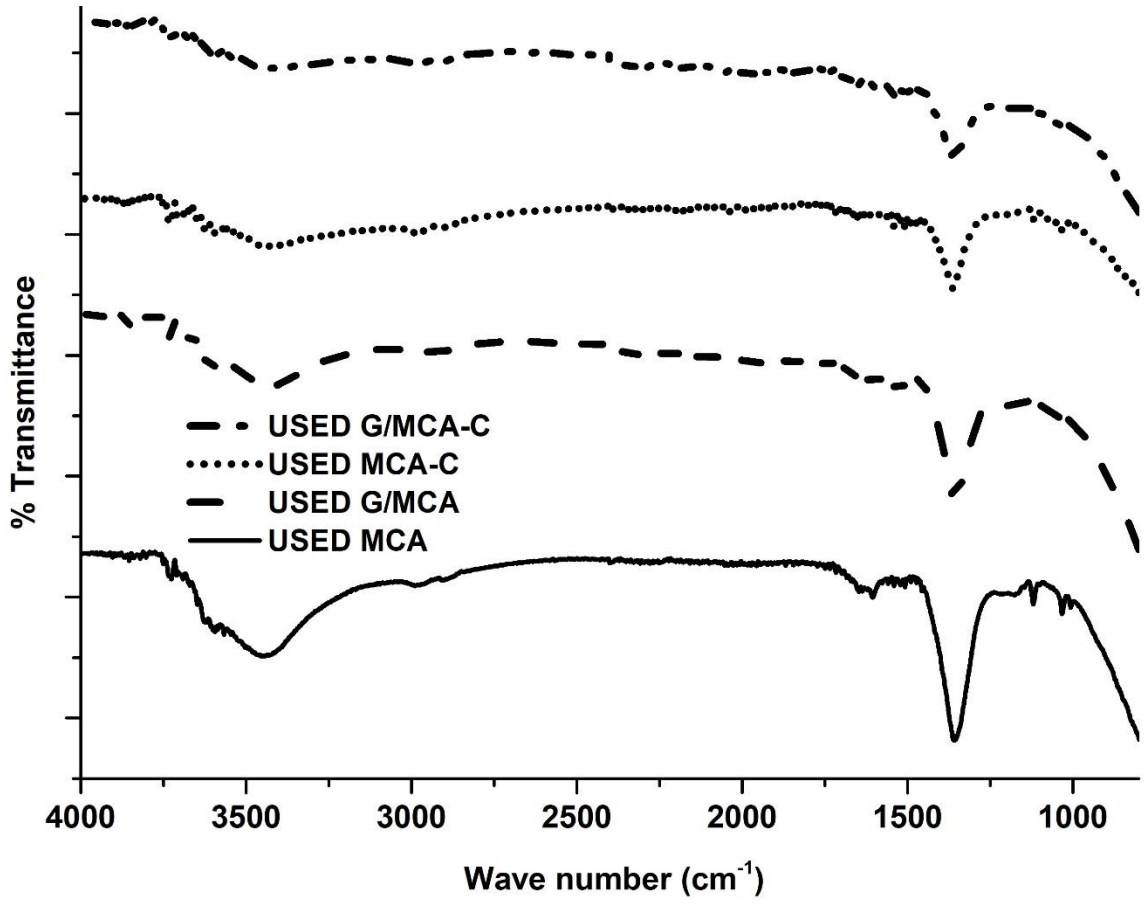

Fig 5.10 FTIR of spent MCA, G/MCA, MCA-C and G/MCA-C

of peaks assigned to the stretching and bending modes of interlayer water molecules is an indication that there was also contribution of hydrogen bonding in the adsorption process [110].

Fig 5.11 shows the XRD of the all the four spent adsorbents. Noticeably, no significant changes were observed in the peak positions of MCA and G/MCA except the changes related to diffractogram peak intensities indicating more random crystal deformation [107, 111].This suggested that anion surface adsorption is one of the mechanism of adsorption as proposed by Wang and his group [112]. The spent MCA-C and G/MCA-C were reconstructed via a memory effect to their respective LDH. It can be construed that intercalation via reconstruction and rehydration play an important role in adsorption of the MO on the surfaces of the MCA-C and G/MCA-C [73]. Hence, the proposed mechanisms of adsorption for MCA and G/MCA are hydrogen bonding, surface adsorption, chemical and electrostatic interactions, while surface reconstruction along with hydrogen bonding, ion exchange, chemical and electrostatic interactions are involved for MCA-C and G/MCA-C.

5.7 Regeneration and reuse of adsorbents

Economic feasibility of an adsorption process is highly influenced by adsorbent regeneration and reuse potentials which could account for saving of up to 70 % of the operation and maintenance costs [82, 83]. To regenerate the adsorbents tested in this study, 0.1 M NaOH slurries of the spent adsorbents were agitated continuously for 24 hours, filtered and washed several times with deionized water. This treatment was used for subsequent regeneration and reuse applications for the three investigated adsorption cycles. Fig 5.12 shows the percentage MO removal for the three adsorption cycles. The percentage

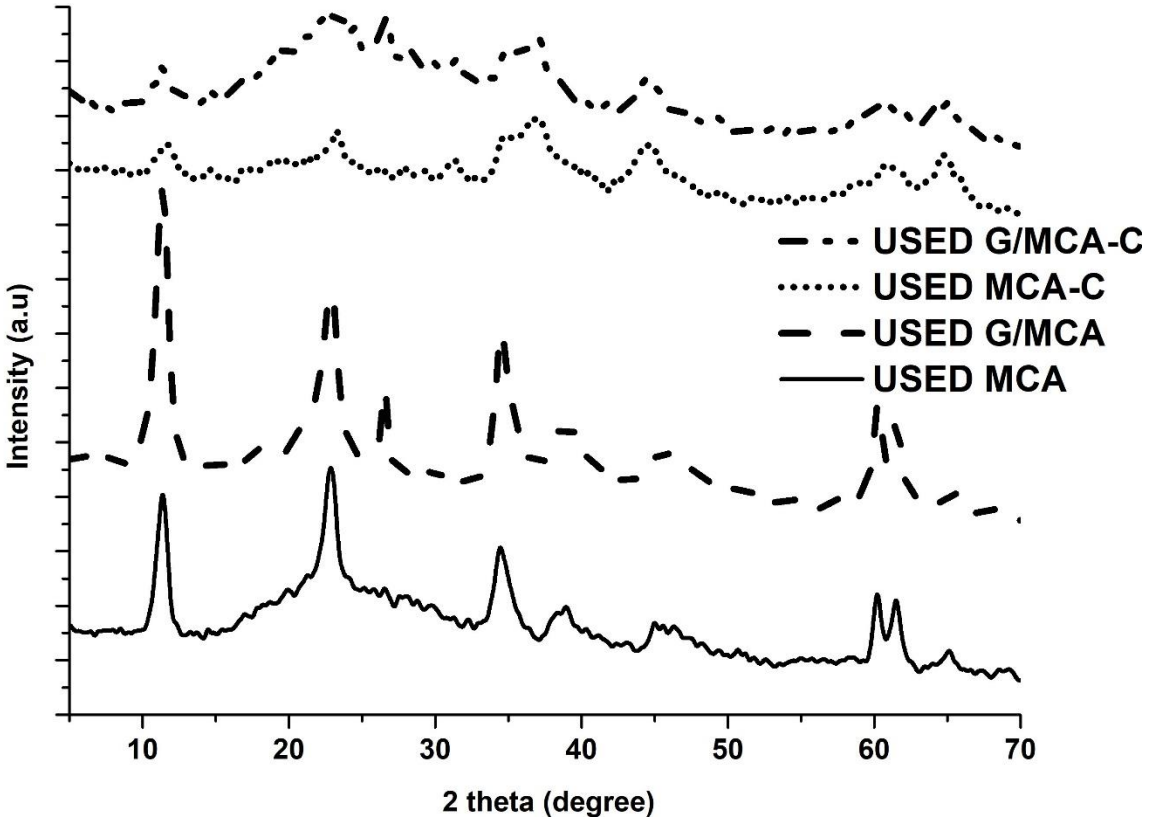

Fig 5.11 XRD of spent MCA, G/MCA, MCA-C and G/MCA-C

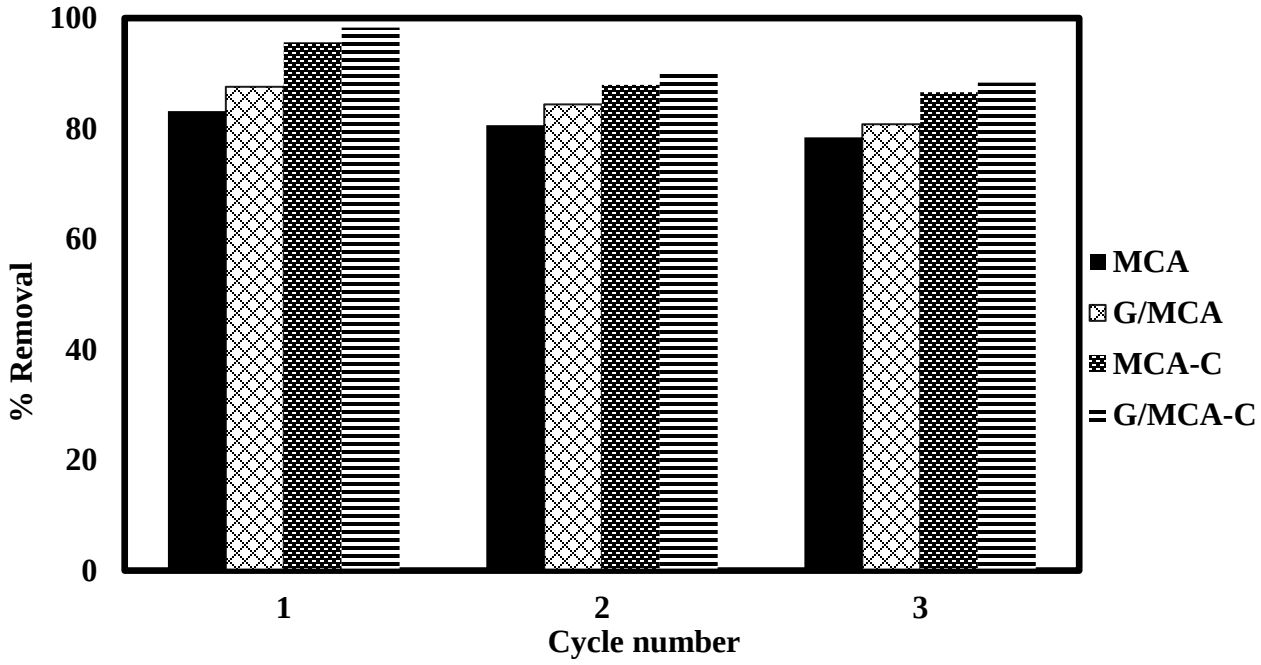

Fig 5.12 Percentage removal of MO dye after three regeneration cycles

removal decreased to 80, 84, 88 and 90 % on the second use for MCA, G/MCA, MCA-C and G/MCA-C, respectively. However, the third reuse showed little reduction in the removal efficiency to 78, 81,87, and 88 %, respectively. This clearly indicates that all the adsorbents employed in this study are characterized by high regeneration and reusability potentials, thereby, showcasing their potentials for cost-effective deployment in the treatment of real water and wastewater for removal of dyes.

5.8 Comparison to other Adsorbents

The performances of the MCA, G/MCA, MCA-C and G/MCA-C adsorbents in terms of the maximum achievable adsorption capacity are compared with other LDH reported in literature as highlighted in Table 4. These tested adsorbent materials perform better than most of the similar reported LDH which buttresses their huge potentials in water treatment applications.

Table 5.4 Comparison of adsorption capacities of LDH for MO adsorption

Adsorbent	**q_m (mg/g)**	**references**
MgNiAl LDH	375	[69]
Glycerine-MgAl LDH	443.5	[106]
Biomorphic MgAl MMO	182.8	[52]
Fe_3O_4/ZnCr	240.16	[44]
MgAl	148	[113]
ZnAl-LDO	181.9	[4]
NiFe	246.91	[98]
Starch-NiFe	387.59	[98]
MCA	357.14	This work
G/MCA	384.62	This work
MCA-C	400.00	This work
G/MCA-C	434.78	This work

CHAPTER 6

CONCLUSION AND RECOMMENDATION

6.1 Conclusion

This work focuses on deployment of adsorption process for water remediation with a focus on dye removal. Layered double hydroxides (LDHs), an anionic clay, was introduced as an adsorbent in use due to its excellent ion exchange capacity and large surface area. This work further reports the synthesis of ternary LDH and its graphene nanocomposite via coprecipitation route and were further calcined at 400^0C for 3h for application in removal of EBT and MO from aqueous phase. Structural characterization of the nanocomposite by FTIR and XRD shows excellent integration of graphene and LDH. The characterization techniques also show the formation of layered double oxide (LDO) after calcination. Parametric study reveals fast sorption process optimized at acidic pH due to abundance of oxygen containing functional groups. It was revealed that adsorption on graphene hybrid is highly pH independent which makes it more promising for industrial application. The adsorption processes were suitably fitted by Langmuir isotherm with maximum adsorption computed to be 384.62 mg/g for EBT adsorption on G/NMA-C and 434.78 mg/g for adsorption of MO on G/NMA-C. The highest capacities obtained for the calcined graphene nanocomposites arise from the synergistic contribution of graphene integration and calcination.

Kinetics study indicates the suitability of pseudo-second order model than pseudo-first order due to chemisorption nature of the adsorption process. Thermodynamics study shows

the exothermic nature of the adsorption with lower adsorption at higher temperature. The adsorption mechanism involves surface adsorption, hydrogen bonding, chemical and electrostatic interaction. The adsorbents are easily recovered with high reusability indicating their potentials for the treatment of dye contaminated water. The calcined graphene hybrid shows superior performance when compared to others due to synergistic effect of hybridization and calcination resulting in large surface area.

6.2 Recommendation

The following are recommended for future study

1. The synthesized materials should be applied to removal of cationic dyes while taking parametric study into consideration.
2. The synthesized materials should be applied to mixture of dyes to investigate simultaneous removability, optimal condition and preference
3. Other forms of nanocomposites such as Graphene/Bentonite/LDH, MWCNT/Bentonite/LDH, bentonite/ ternary LDH should be synthesized and their performance tested on both cationic and anionic dyes
4. The synthesized and recommended hybrids should be used in removal of heavy metals from aqueous phase
5. The synthesized and recommended hybrids should be tested in other purification schemes such desulfurization of wastewater and allied processes

References

[1] M. Hasmath Farzana and S. Meenakshi, "Decolorization and detoxification of Acid blue 158 dye using cuttlefish bone powder as co-adsorbent via photocatalytic method," *Journal of Water Process Engineering,* vol. 2, pp. 22-30, 2014/06/01/ 2014.

[2] E. Akceylan, M. Bahadir, and M. Yılmaz, "Removal efficiency of a calix[4]arene-based polymer for water-soluble carcinogenic direct azo dyes and aromatic amines," *Journal of Hazardous Materials,* vol. 162, pp. 960-966, 2009/03/15/ 2009.

[3] S. N. Jain and P. R. Gogate, "Acid Blue 113 removal from aqueous solution using novel biosorbent based on NaOH treated and surfactant modified fallen leaves of Prunus Dulcis," *Journal of Environmental Chemical Engineering,* vol. 5, pp. 3384-3394, 2017/08/01/ 2017.

[4] Q. Hu, Z. Xu, S. Qiao, F. Haghseresht, M. Wilson, and G. Q. Lu, "A novel color removal adsorbent from heterocoagulation of cationic and anionic clays," *Journal of colloid and interface science,* vol. 308, pp. 191-199, 2007.

[5] R. A. K. Rao, S. Ikram, and M. K. Uddin, "Removal of Cr (VI) from aqueous solution on seeds of Artimisia absinthium (novel plant material)," *Desalination and Water Treatment,* vol. 54, pp. 3358-3371, 2015.

[6] R. A. K. Rao, S. Ikram, and M. K. Uddin, "Removal of Cd (II) from aqueous solution by exploring the biosorption characteristics of gaozaban (Onosma bracteatum)," *Journal of Environmental Chemical Engineering,* vol. 2, pp. 1155-1164, 2014.

[7] R. A. K. Rao and M. Kashifuddin, "Kinetics and isotherm studies of Cd (II) adsorption from aqueous solution utilizing seeds of bottlebrush plant (Callistemon chisholmii)," *Applied Water Science,* vol. 4, pp. 371-383, 2014.

[8] R. A. K. Rao and M. Kashifuddin, "Adsorption properties of coriander seed powder (Coriandrum sativum): Extraction and pre-concentration of Pb (II), Cu (II) and Zn (II) ions from aqueous solution," *Adsorption Science & Technology,* vol. 30, pp. 127-146, 2012.

[9] M. A. Khan, M. K. Uddin, R. Bushra, A. Ahmad, and S. A. Nabi, "Synthesis and characterization of polyaniline Zr (IV) molybdophosphate for the adsorption of phenol from aqueous solution," *Reaction Kinetics, Mechanisms and Catalysis,* vol. 113, pp. 499-517, 2014.

[10] C. Lei, X. Zhu, B. Zhu, C. Jiang, Y. Le, and J. Yu, "Superb adsorption capacity of hierarchical calcined Ni/Mg/Al layered double hydroxides for Congo red and Cr(VI) ions," *Journal of Hazardous Materials,* vol. 321, pp. 801-811, 1/5/ 2017.

[11] N. N. Das, J. Konar, M. K. Mohanta, and S. C. Srivastava, "Adsorption of Cr(VI) and Se(IV) from their aqueous solutions onto Zr4+-substituted ZnAl/MgAl-layered double hydroxides: effect of Zr4+ substitution in the layer," *Journal of Colloid and Interface Science,* vol. 270, pp. 1-8, 2004/02/01/ 2004.

[12] M. Zubair, M. Daud, G. McKay, F. Shehzad, and M. A. Al-Harthi, "Recent progress in layered double hydroxides (LDH)-containing hybrids as adsorbents for water remediation," *Applied Clay Science,* vol. 143, pp. 279-292, 2017.

[13] M. Daud, M. S. Kamal, F. Shehzad, and M. A. Al-Harthi, "Graphene/layered double hydroxides nanocomposites: A review of recent progress in synthesis and applications," *Carbon*, vol. 104, pp. 241-252, 2016.
[14] D. G. Evans and R. C. Slade, "Structural aspects of layered double hydroxides," in *Layered double hydroxides*, ed: Springer, 2006, pp. 1-87.
[15] K.-H. Goh, T.-T. Lim, and Z. Dong, "Application of layered double hydroxides for removal of oxyanions: a review," *Water research*, vol. 42, pp. 1343-1368, 2008.
[16] F. Li and X. Duan, "Applications of layered double hydroxides," in *Layered double hydroxides*, ed: Springer, 2006, pp. 193-223.
[17] M. Sajid and C. Basheer, "Layered double hydroxides: Emerging sorbent materials for analytical extractions," *TrAC Trends in Analytical Chemistry*, vol. 75, pp. 174-182, 2016.
[18] A. Marchi and C. Apesteguıa, "Impregnation-induced memory effect of thermally activated layered double hydroxides," *Applied Clay Science*, vol. 13, pp. 35-48, 1998.
[19] A. Besserguenev, A. Fogg, R. Francis, S. Price, D. O'hare, V. Isupov, *et al.*, "Synthesis and Structure of the Gibbsite Intercalation Compounds [LiAl2 (OH) 6] X {X= Cl, Br, NO3} and [LiAl2 (OH) 6] Cl⊙ H2O Using Synchrotron X-ray and Neutron Powder Diffraction," *Chemistry of Materials*, vol. 9, pp. 241-247, 1997.
[20] K. Muramatsu, O. Saber, and H. Tagaya, "Preparation of new layered double hydroxide, Zn-Mo LDH," *Journal of Porous Materials*, vol. 14, pp. 481-484, 2007.
[21] O. Saber, B. Hatano, and H. Tagaya, "Preparation of New Layered Double Hydroxide, Co-TiLDH," *Journal of inclusion phenomena and macrocyclic chemistry*, vol. 51, pp. 17-25, 2005.
[22] O. Saber and H. Tagaya, "New layered double hydroxide, Zn–Ti LDH: preparation and intercalation reactions," *Journal of inclusion phenomena and macrocyclic chemistry*, vol. 45, pp. 107-115, 2003.
[23] M. Shao, M. Wei, D. G. Evans, and X. Duan, "Hierarchical Structures Based on Functionalized Magnetic Cores and Layered Double-Hydroxide Shells: Concept, Controlled Synthesis, and Applications," *Chemistry–A European Journal*, vol. 19, pp. 4100-4108, 2013.
[24] B. Bi, L. Xu, B. Xu, and X. Liu, "Heteropoly blue-intercalated layered double hydroxides for cationic dye removal from aqueous media," *Applied Clay Science*, vol. 54, pp. 242-247, 2011.
[25] J. He, M. Wei, B. Li, Y. Kang, D. G. Evans, and X. Duan, "Preparation of layered double hydroxides," in *Layered double hydroxides*, ed: Springer, 2006, pp. 89-119.
[26] K. L. Erickson, T. E. Bostrom, and R. L. Frost, "A study of structural memory effects in synthetic hydrotalcites using environmental SEM," *Materials Letters*, vol. 59, pp. 226-229, 2005.
[27] Y. Zhao, F. Li, R. Zhang, D. G. Evans, and X. Duan, "Preparation of layered double-hydroxide nanomaterials with a uniform crystallite size using a new method involving separate nucleation and aging steps," *Chemistry of Materials*, vol. 14, pp. 4286-4291, 2002.
[28] N. Morel-Desrosiers, J. Pisson, Y. Israëli, C. Taviot-Guého, J.-P. Besse, and J.-P. Morel, "Intercalation of dicarboxylate anions into a Zn–Al–Cl layered double

hydroxide: microcalorimetric determination of the enthalpies of anion exchange," *Journal of Materials Chemistry,* vol. 13, pp. 2582-2585, 2003.

[29] Z.-q. Zhang, M.-c. Liao, H.-Y. Zeng, S. Xu, X.-j. Liu, J.-z. Du, *et al.*, "Temperature effect on chromium(VI) removal by Mg/Al mixed metal oxides as adsorbents," *Applied Clay Science,* vol. 102, pp. 246-253, 12// 2014.

[30] M. Ogawa and H. Kaiho, "Homogeneous precipitation of uniform hydrotalcite particles," *Langmuir,* vol. 18, pp. 4240-4242, 2002.

[31] L. Shao, Y. Yao, S. Quan, H. Wei, R. Wang, and Z. Guo, "One-pot in situ synthesized TiO 2/layered double hydroxides (LDHs) composites toward environmental remediation," *Materials Letters,* vol. 114, pp. 111-114, 2014.

[32] M. Zubair, N. Jarrah, M. S. Manzar, M. Al-Harthi, M. Daud, N. D. Mu'azu, *et al.*, "Adsorption of eriochrome black T from aqueous phase on MgAl-, CoAl- and NiFe- calcined layered double hydroxides: Kinetic, equilibrium and thermodynamic studies," *Journal of Molecular Liquids,* vol. 230, pp. 344-352, 3// 2017.

[33] R.-r. Shan, L.-g. Yan, Y.-m. Yang, K. Yang, S.-j. Yu, H.-q. Yu, *et al.*, "Highly efficient removal of three red dyes by adsorption onto Mg–Al-layered double hydroxide," *Journal of Industrial and Engineering Chemistry,* vol. 21, pp. 561-568, 1/25/ 2015.

[34] D. Chen, Y. Li, J. Zhang, J.-z. Zhou, Y. Guo, and H. Liu, "Magnetic Fe 3 O 4/ZnCr-layered double hydroxide composite with enhanced adsorption and photocatalytic activity," *Chemical Engineering Journal,* vol. 185, pp. 120-126, 2012.

[35] G. Huang, Y. Sun, C. Zhao, Y. Zhao, Z. Song, J. Chen, *et al.*, "Water–n-BuOH solvothermal synthesis of ZnAl–LDHs with different morphologies and its calcined product in efficient dyes removal," *Journal of Colloid and Interface Science,* vol. 494, pp. 215-222, 2017.

[36] Y. X. Zhang, X. D. Hao, M. Kuang, H. Zhao, and Z. Q. Wen, "Preparation, characterization and dye adsorption of Au nanoparticles/ZnAl layered double oxides nanocomposites," *Applied Surface Science,* vol. 283, pp. 505-512, 2013.

[37] Y.-M. Zheng, N. Li, and W.-D. Zhang, "Preparation of nanostructured microspheres of Zn–Mg–Al layered double hydroxides with high adsorption property," *Colloids and Surfaces A: Physicochemical and Engineering Aspects,* vol. 415, pp. 195-201, 2012.

[38] P.-P. Huang, C.-Y. Cao, F. Wei, Y.-B. Sun, and W.-G. Song, "MgAl layered double hydroxides with chloride and carbonate ions as interlayer anions for removal of arsenic and fluoride ions in water," *RSC Advances,* vol. 5, pp. 10412-10417, 2015.

[39] Y. Yasin, M. Mohamad, A. Saad, A. Sanusi, and F. H. Ahmad, "Removal of lead ions from aqueous solutions using intercalated tartrate-Mg–Al layered double hydroxides," *Desalination and Water Treatment,* vol. 52, pp. 4266-4272, 2014.

[40] X. Yue, W. Liu, Z. Chen, and Z. Lin, "Simultaneous removal of Cu (II) and Cr (VI) by Mg–Al–Cl layered double hydroxide and mechanism insight," *Journal of Environmental Sciences,* 2016.

[41] R. Lafi, K. Charradi, M. A. Djebbi, A. B. H. Amara, and A. Hafiane, "Adsorption study of Congo red dye from aqueous solution to Mg–Al–layered double hydroxide," *Advanced Powder Technology,* vol. 27, pp. 232-237, 2016.

[42] B. Li, Y. Zhang, X. Zhou, Z. Liu, Q. Liu, and X. Li, "Different dye removal mechanisms between monodispersed and uniform hexagonal thin plate-like MgAl–CO 3 2--LDH and its calcined product in efficient removal of Congo red from water," *Journal of Alloys and Compounds*, vol. 673, pp. 265-271, 2016.
[43] P. Monash and G. Pugazhenthi, "Utilization of calcined Ni-Al layered double hydroxide (LDH) as an Adsorbent for removal of methyl orange dye from aqueous solution," *Environmental Progress & Sustainable Energy*, vol. 33, pp. 154-159, 2014.
[44] D. Chen, Y. Li, J. Zhang, W. Li, J. Zhou, L. Shao, *et al.*, "Efficient removal of dyes by a novel magnetic Fe 3 O 4/ZnCr-layered double hydroxide adsorbent from heavy metal wastewater," *Journal of hazardous materials*, vol. 243, pp. 152-160, 2012.
[45] J. Liu, X. Li, J. Luo, C. Duan, H. Hu, and G. Qian, "Enhanced decolourisation of methylene blue by LDH-bacteria aggregates with bioregeneration," *Chemical Engineering Journal*, vol. 242, pp. 187-194, 2014.
[46] M. Sui, Y. Zhou, L. Sheng, and B. Duan, "Adsorption of norfloxacin in aqueous solution by Mg–Al layered double hydroxides with variable metal composition and interlayer anions," *Chemical engineering journal*, vol. 210, pp. 451-460, 2012.
[47] K. Xing, H. Wang, L. Guo, W. Song, and Z. Zhao, "Adsorption of tripolyphosphate from aqueous solution by Mg–Al–CO 3-layered double hydroxides," *Colloids and Surfaces A: Physicochemical and Engineering Aspects*, vol. 328, pp. 15-20, 2008.
[48] F. Yang, S. Sun, X. Chen, Y. Chang, F. Zha, and Z. Lei, "Mg–Al layered double hydroxides modified clay adsorbents for efficient removal of Pb2 +, Cu2 + and Ni2 + from water," *Applied Clay Science*, vol. 123, pp. 134-140, 4// 2016.
[49] Y. Yasin, A. H. Abdul Malek, and S. Mariam Sumari, "Adsorption of eriochrome black dye from aqueous solution onto anionic layered double hydroxides," *Oriental Journal of Chemistry*, vol. 26, p. 1293, 2010.
[50] I. Ahmed and M. Gasser, "Adsorption study of anionic reactive dye from aqueous solution to Mg–Fe–CO 3 layered double hydroxide (LDH)," *Applied Surface Science*, vol. 259, pp. 650-656, 2012.
[51] M. K. Uddin, "A review on the adsorption of heavy metals by clay minerals, with special focus on the past decade," *Chemical Engineering Journal*, vol. 308, pp. 438-462, 2017.
[52] L. Gao, Q. Li, X. Hu, X. Wang, H. Song, L. Yan, *et al.*, "One-pot synthesis of biomorphic Mg-Al mixed metal oxides with enhanced methyl orange adsorption properties," *Applied Clay Science*, vol. 126, pp. 299-305, 2016.
[53] L. Yang, Z. Shahrivari, P. K. Liu, M. Sahimi, and T. T. Tsotsis, "Removal of trace levels of arsenic and selenium from aqueous solutions by calcined and uncalcined layered double hydroxides (LDH)," *Industrial & Engineering Chemistry Research*, vol. 44, pp. 6804-6815, 2005.
[54] N. Das, J. Konar, M. Mohanta, and S. Srivastava, "Adsorption of Cr (VI) and Se (IV) from their aqueous solutions onto Zr 4+-substituted ZnAl/MgAl-layered double hydroxides: effect of Zr 4+ substitution in the layer," *Journal of colloid and interface science*, vol. 270, pp. 1-8, 2004.
[55] S. Tezuka, R. Chitrakar, K. Sakane, A. Sonoda, K. Ooi, and T. Tomida, "The synthesis and phosphate adsorptive properties of Mg (II)–Mn (III) layered double

hydroxides and their heat-treated materials," *Bulletin of the Chemical Society of Japan*, vol. 77, pp. 2101-2107, 2004.
[56] M. Dadwhal, M. Sahimi, and T. T. Tsotsis, "Adsorption isotherms of arsenic on conditioned layered double hydroxides in the presence of various competing ions," *Industrial & Engineering Chemistry Research*, vol. 50, pp. 2220-2226, 2011.
[57] M. Temkin and V. Pyzhev, "Recent modifications to Langmuir isotherms," 1940.
[58] H. Javadian, "Application of kinetic, isotherm and thermodynamic models for the adsorption of Co (II) ions on polyaniline/polypyrrole copolymer nanofibers from aqueous solution," *Journal of Industrial and Engineering Chemistry*, vol. 20, pp. 4233-4241, 2014.
[59] V. Vimonses, S. Lei, B. Jin, C. W. Chow, and C. Saint, "Kinetic study and equilibrium isotherm analysis of Congo Red adsorption by clay materials," *Chemical Engineering Journal*, vol. 148, pp. 354-364, 2009.
[60] H. Chen, J. Zhao, J. Wu, and G. Dai, "Isotherm, thermodynamic, kinetics and adsorption mechanism studies of methyl orange by surfactant modified silkworm exuviae," *Journal of hazardous materials*, vol. 192, pp. 246-254, 2011.
[61] O. Redlich and D. L. Peterson, "A useful adsorption isotherm," *Journal of Physical Chemistry*, vol. 63, pp. 1024-1024, 1959.
[62] R. Zandipak and S. Sobhanardakani, "Synthesis of NiFe2O4 nanoparticles for removal of anionic dyes from aqueous solution," *Desalination and Water Treatment*, vol. 57, pp. 11348-11360, 2016.
[63] N. B.-H. Abdelkader, A. Bentouami, Z. Derriche, N. Bettahar, and L.-C. De Menorval, "Synthesis and characterization of Mg–Fe layer double hydroxides and its application on adsorption of Orange G from aqueous solution," *Chemical Engineering Journal*, vol. 169, pp. 231-238, 2011.
[64] C. Qi, J. Amphlett, and B. A. Peppley, "Product composition as a function of temperature over NiAl-layered double hydroxide derived catalysts in steam reforming of methanol," *Applied Catalysis A: General*, vol. 302, pp. 237-243, 2006.
[65] J. Pérez-Ramírez, S. Abelló, and N. M. van der Pers, "Influence of the divalent cation on the thermal activation and reconstruction of hydrotalcite-like compounds," *The Journal of Physical Chemistry C*, vol. 111, pp. 3642-3650, 2007.
[66] M. Gasser, "Inorganic layered double hydroxides as ascorbic acid (vitamin c) delivery system—Intercalation and their controlled release properties," *Colloids and Surfaces B: Biointerfaces*, vol. 73, pp. 103-109, 2009.
[67] M.-X. Zhu, Y.-P. Li, M. Xie, and H.-Z. Xin, "Sorption of an anionic dye by uncalcined and calcined layered double hydroxides: a case study," *Journal of hazardous materials*, vol. 120, pp. 163-171, 2005.
[68] L.-g. Yan, K. Yang, R.-r. Shan, T. Yan, J. Wei, S.-j. Yu, *et al.*, "Kinetic, isotherm and thermodynamic investigations of phosphate adsorption onto core–shell Fe3O4@LDHs composites with easy magnetic separation assistance," *Journal of Colloid and Interface Science*, vol. 448, pp. 508-516, 6/15/ 2015.
[69] H. Zaghouane-Boudiaf, M. Boutahala, and L. Arab, "Removal of methyl orange from aqueous solution by uncalcined and calcined MgNiAl layered double hydroxides (LDHs)," *Chemical Engineering Journal*, vol. 187, pp. 142-149, 2012.
[70] D. Iruretagoyena Ferrer, "Layered Double Hydroxides Supported on Graphene Oxide for CO2 Adsorption," in *Supported Layered Double Hydroxides as CO2*

Adsorbents for Sorption-enhanced H2 Production, ed Cham: Springer International Publishing, 2016, pp. 85-113.

[71] O. Clause, M. G. Coelho, M. Gazzano, D. Matteuzzi, F. Trifiro, and A. Vaccari, "Synthesis and thermal reactivity of nickel-containing anionic clays," *Applied clay science,* vol. 8, pp. 169-186, 1993.

[72] W. T. Reichle, "Synthesis of anionic clay minerals (mixed metal hydroxides, hydrotalcite)," *Solid State Ionics,* vol. 22, pp. 135-141, 1986.

[73] S. M. Sumari, Z. Hamzah, and N. Kantasamy, "ADSORPTION OF ANIONIC DYES FROM AQUEOUS SOLUTIONS BY CALCINED AND UNCALCINED Mg/Al LAYERED DOUBLE HYDROXIDE," *Malaysian Journal of Analytical Sciences,* vol. 20, pp. 777-792, 2016.

[74] M. N. Pahalagedara, M. Samaraweera, S. Dharmarathna, C.-H. Kuo, L. R. Pahalagedara, J. A. Gascón, *et al.*, "Removal of azo dyes: intercalation into sonochemically synthesized NiAl layered double hydroxide," *The Journal of Physical Chemistry C,* vol. 118, pp. 17801-17809, 2014.

[75] J. Das, B. Patra, N. Baliarsingh, and K. Parida, "Adsorption of phosphate by layered double hydroxides in aqueous solutions," *Applied Clay Science,* vol. 32, pp. 252-260, 2006.

[76] Z.-M. Ni, S.-J. Xia, L.-G. Wang, F.-F. Xing, and G.-X. Pan, "Treatment of methyl orange by calcined layered double hydroxides in aqueous solution: adsorption property and kinetic studies," *Journal of Colloid and Interface Science,* vol. 316, pp. 284-291, 2007.

[77] L. Deng, Z. Shi, X. Peng, and S. Zhou, "Magnetic calcinated cobalt ferrite/magnesium aluminum hydrotalcite composite for enhanced adsorption of methyl orange," *Journal of Alloys and Compounds,* vol. 688, pp. 101-112, 2016.

[78] M. Ahmed and A. Mohamed, "An efficient adsorption of indigo carmine dye from aqueous solution on mesoporous Mg/Fe layered double hydroxide nanoparticles prepared by controlled sol-gel route," *Chemosphere,* vol. 174, pp. 280-288, 2017.

[79] X. Yuan, Y. Wang, J. Wang, C. Zhou, Q. Tang, and X. Rao, "Calcined graphene/MgAl-layered double hydroxides for enhanced Cr (VI) removal," *Chemical engineering journal,* vol. 221, pp. 204-213, 2013.

[80] J. Ma, F. Yu, L. Zhou, L. Jin, M. Yang, J. Luan, *et al.*, "Enhanced adsorptive removal of methyl orange and methylene blue from aqueous solution by alkali-activated multiwalled carbon nanotubes," *ACS applied materials & interfaces,* vol. 4, pp. 5749-5760, 2012.

[81] R. Extremera, I. Pavlovic, M. Pérez, and C. Barriga, "Removal of acid orange 10 by calcined Mg/Al layered double hydroxides from water and recovery of the adsorbed dye," *Chemical engineering journal,* vol. 213, pp. 392-400, 2012.

[82] P. Ganesan, R. Kamaraj, and S. Vasudevan, "Application of isotherm, kinetic and thermodynamic models for the adsorption of nitrate ions on graphene from aqueous solution," *Journal of the Taiwan Institute of Chemical Engineers,* vol. 44, pp. 808-814, 2013.

[83] S. Samuei, Z. Rezvani, and A. R. Amani-Ghadim, "Comparative study of removal of reactive dye by LDHs: The effect of cation variety," *Environmental Progress & Sustainable Energy,* vol. 36, pp. 372-381, 2017.

[84] F. A. Ngwabebhoh, M. Gazi, and A. A. Oladipo, "Adsorptive removal of multi-azo dye from aqueous phase using a semi-IPN superabsorbent chitosan-starch hydrogel," *Chemical Engineering Research and Design,* vol. 112, pp. 274-288, 2016.

[85] A. Mittal and V. K. Gupta, "Adsorptive removal and recovery of the azo dye Eriochrome Black T," *Toxicological and Environ Chemistry,* vol. 92, pp. 1813-1823, 2010.

[86] M. D. G. de Luna, E. D. Flores, D. A. D. Genuino, C. M. Futalan, and M.-W. Wan, "Adsorption of Eriochrome Black T (EBT) dye using activated carbon prepared from waste rice hulls—optimization, isotherm and kinetic studies," *Journal of the Taiwan Institute of Chemical Engineers,* vol. 44, pp. 646-653, 2013.

[87] Ö. Şahin, C. Saka, and S. Kutluay, "Cold plasma and microwave radiation applications on almond shell surface and its effects on the adsorption of Eriochrome Black T," *Journal of Industrial and Engineering Chemistry,* vol. 19, pp. 1617-1623, 2013.

[88] P. N. Dave, S. Kaur, and E. Khosla, "Removal of Eriochrome black-T by adsorption on to eucalyptus bark using green technology," 2011.

[89] V. M. Vučurović, R. N. Razmovski, U. D. Miljić, and V. S. Puškaš, "Removal of cationic and anionic azo dyes from aqueous solutions by adsorption on maize stem tissue," *Journal of the Taiwan Institute of Chemical Engineers,* vol. 45, pp. 1700-1708, 2014.

[90] T. P. F. Teixeira, S. Aquino, S. Pereira, and A. Dias, "Use of calcined layered double hydroxides for the removal of color and organic matter from textile effluents: kinetic, equilibrium and recycling studies," *Brazilian Journal of Chemical Engineering,* vol. 31, pp. 19-26, 2014.

[91] D. Bharali, R. Devi, P. Bharali, and R. C. Deka, "Synthesis of high surface area mixed metal oxide from the NiMgAl LDH precursor for nitro-aldol condensation reaction," *New Journal of Chemistry,* vol. 39, pp. 172-178, 2015.

[92] S. Tang and H. K. Lee, "Application of Dissolvable Layered Double Hydroxides As Sorbent in Dispersive Solid-Phase Extraction and Extraction by Co-Precipitation for the Determination of Aromatic Acid Anions," *Analytical Chemistry,* vol. 85, pp. 7426-7433, 2013/08/06 2013.

[93] S. Roy, S. K. Srivastava, J. Pionteck, and V. Mittal, "Mechanically and Thermally Enhanced Multiwalled Carbon Nanotube–Graphene Hybrid filled Thermoplastic Polyurethane Nanocomposites," *Macromolecular Materials and Engineering,* vol. 300, pp. 346-357, 2015.

[94] M. G. Álvarez, D. Tichit, F. Medina, and J. Llorca, "Role of the synthesis route on the properties of hybrid LDH-graphene as basic catalysts," *Applied Surface Science,* vol. 396, pp. 821-831, 2017/02/28/ 2017.

[95] A. Garcia-Gallastegui, D. Iruretagoyena, V. Gouvea, M. Mokhtar, A. M. Asiri, S. N. Basahel, *et al.*, "Graphene Oxide as Support for Layered Double Hydroxides: Enhancing the CO2 Adsorption Capacity," *Chemistry of Materials,* vol. 24, pp. 4531-4539, 2012/12/11 2012.

[96] S. Mallakpour and M. Dinari, "Hybrids of Mg–Al-layered double hydroxide and multiwalled carbon nanotube as a reinforcing filler in the l-phenylalanine-based

polymer nanocomposites," *Journal of Thermal Analysis and Calorimetry*, vol. 119, pp. 1905-1912, March 01 2015.

[97] S. Yang, L. Wang, X. Zhang, W. Yang, and G. Song, "Enhanced adsorption of Congo red dye by functionalized carbon nanotube/mixed metal oxides nanocomposites derived from layered double hydroxide precursor," *Chemical Engineering Journal,* vol. 275, pp. 315-321, 2015/09/01/ 2015.

[98] M. Zubair, N. Jarrah, Ihsanullah, A. Khalid, M. S. Manzar, T. S. Kazeem, *et al.*, "Starch-NiFe-layered double hydroxide composites: Efficient removal of methyl orange from aqueous phase," *Journal of Molecular Liquids,* vol. 249, pp. 254-264, 1// 2018.

[99] D. Chebli, A. Bouguettoucha, A. Reffas, C. Tiar, M. Boutahala, H. Gulyas, *et al.*, "Removal of the anionic dye Biebrich scarlet from water by adsorption to calcined and non-calcined Mg–Al layered double hydroxides," *Desalination and Water Treatment,* vol. 57, pp. 22061-22073, 2016.

[100] K. El Hassani, B. H. Beakou, D. Kalnina, E. Oukani, and A. Anouar, "Effect of morphological properties of layered double hydroxides on adsorption of azo dye Methyl Orange: A comparative study," *Applied Clay Science,* vol. 140, pp. 124-131, 2017/05/01/ 2017.

[101] Y. Lu, B. Jiang, L. Fang, F. Ling, J. Gao, F. Wu, *et al.*, "High performance NiFe layered double hydroxide for methyl orange dye and Cr (VI) adsorption," *Chemosphere,* vol. 152, pp. 415-422, 2016.

[102] Y. S. Ho and G. McKay, "Pseudo-second order model for sorption processes," *Process Biochemistry,* vol. 34, pp. 451-465, 1999/07/01/ 1999.

[103] X. Xin, W. Si, Z. Yao, R. Feng, B. Du, L. Yan, *et al.*, "Adsorption of benzoic acid from aqueous solution by three kinds of modified bentonites," *Journal of Colloid and Interface Science,* vol. 359, pp. 499-504, 2011/07/15/ 2011.

[104] R.-r. Shan, L.-g. Yan, K. Yang, S.-j. Yu, Y.-f. Hao, H.-q. Yu, *et al.*, "Magnetic Fe3O4/MgAl-LDH composite for effective removal of three red dyes from aqueous solution," *Chemical Engineering Journal,* vol. 252, pp. 38-46, 2014/09/15/ 2014.

[105] A. Khalid, M. Zubair, and Ihsanullah, "A Comparative Study on the Adsorption of Eriochrome Black T Dye from Aqueous Solution on Graphene and Acid-Modified Graphene," *Arabian Journal for Science and Engineering,* April 25 2017.

[106] W. Yao, S. Yu, J. Wang, Y. Zou, S. Lu, Y. Ai, *et al.*, "Enhanced removal of methyl orange on calcined glycerol-modified nanocrystallined Mg/Al layered double hydroxides," *Chemical Engineering Journal,* vol. 307, pp. 476-486, 2017/01/01/ 2017.

[107] J. Wang, D. Kang, X. Yu, M. Ge, and Y. Chen, "Synthesis and characterization of Mg–Fe–La trimetal composite as an adsorbent for fluoride removal," *Chemical Engineering Journal,* vol. 264, pp. 506-513, 2015/03/15/ 2015.

[108] Q. Zhou, F. Chen, W. Wu, R. Bu, W. Li, and F. Yang, "Reactive orange 5 removal from aqueous solution using hydroxyl ammonium ionic liquids/layered double hydroxides intercalation composites," *Chemical Engineering Journal,* vol. 285, pp. 198-206, 2016.

[109] N. Dizge, C. Aydiner, E. Demirbas, M. Kobya, and S. Kara, "Adsorption of reactive dyes from aqueous solutions by fly ash: Kinetic and equilibrium studies," *Journal of Hazardous Materials,* vol. 150, pp. 737-746, 2008/02/11/ 2008.

[110] Z. Jin, X. Wang, Y. Sun, Y. Ai, and X. Wang, "Adsorption of 4-n-Nonylphenol and Bisphenol-A on Magnetic Reduced Graphene Oxides: A Combined Experimental and Theoretical Studies," *Environmental Science & Technology*, vol. 49, pp. 9168-9175, 2015/08/04 2015.
[111] W. Xiang, G. Zhang, Y. Zhang, D. Tang, and J. Wang, "Synthesis and characterization of cotton-like Ca–Al–La composite as an adsorbent for fluoride removal," *Chemical Engineering Journal*, vol. 250, pp. 423-430, 2014/08/15/ 2014.
[112] S. L. Wang, R. J. Hseu, R. R. Chang, P. N. Chiang, J. H. Chen, and Y. M. Tzou, "Adsorption and thermal desorption of Cr(VI) on Li/Al layered double hydroxide," *Colloids and Surfaces A: Physicochemical and Engineering Aspects*, vol. 277, pp. 8-14, 2006/04/05/ 2006.
[113] L. Ai, C. Zhang, and L. Meng, "Adsorption of Methyl Orange from Aqueous Solution on Hydrothermal Synthesized Mg–Al Layered Double Hydroxide," *Journal of Chemical & Engineering Data*, vol. 56, pp. 4217-4225, 2011/11/10 2011.

Vitae

Name : Taye Saheed Kazeem

Nationality : Nigerian

Date of Birth :8/9/1988

Email : kazeemts@gmail.com

Address : 86, Yaya Abatan street, Ogba-ijaiye, Lagos -100218, Nigeria

Academic Background :B.Sc Chemical Engineering (2008-2013), First class honors

Obafemi Awolowo University, Ile-Ife, Nigeria

Research Interest

- Nanomaterials synthesis
- Novel hybrid fabrication and characterization
- Wastewater treatment
- Renewable energy, thermal energy storage materials and phase change materials

Publications

- Zubair, M.; Jarrah, N.; Ihsanullah; Khalid, A.; Manzar, M. S.; Kazeem, T. S.; Al-Harthi, M. A., Starch-NiFe-layered double hydroxide composites: Efficient removal of methyl orange from aqueous phase. *Journal of Molecular Liquids* **2018,** *249*, 254-264. https://www.sciencedirect.com/science/article/pii/S0167732217338631 (**Impact factor: 3.648**)
- Mu'azu, N. D.; Jarrah, N.; Kazeem, T. S.; Zubair, M.; Al-Harthi, M., Bentonite-layered double hydroxide composite for enhanced aqueous adsorption of Eriochrome Black T. *Applied Clay Science* **2018,** *161*, 23-34. https://www.sciencedirect.com/science/article/pii/S0169131718301595 (**Impact factor: 3.101**)